Solid-state 95Mo NMR study of (aryldiazenido)- and (organohydrazido)polyoxomolybdates. Investigation of model compounds of catalytic molybdenum environments

ARTICLE *in* INORGANIC CHEMISTRY · SEPTEMBER 1990

Impact Factor: 4.76 · DOI: 10.1021/ic00343a024

Reaction of *trans*-1,2-Bis((diphenylphosphino)methyl)cyclopropane with *cis*-(Piperidine)$_2$Mo(CO)$_4$. A solution of **1** (0.31 g, 0.71 mmol) and *cis*-(piperidine)$_2$Mo(CO)$_4$[9] (0.25 g, 0.66 mmol) in 20 mL of CH_2Cl_2 was stirred for 1.5 h. Solvent was evaporated under vacuum. The resulting oil was dissolved in 10 mL of Et_2O, and the mixture was filtered. Solvent was evaporated under vacuum to yield the oligomeric mixture **4** (366 mg) as a light yellow solid: $^{31}P\{^1H\}$ NMR (CD_2Cl_2) δ 34.3 (s); IR (CH_2Cl_2) 2015 (m), 1917 (sh), 1890 (s), 1844 (m) cm^{-1}.

The average molecular weight of the oligomeric mixture **4** was determined by the isopiestic method using a Signer-type apparatus.[16] **4** (0.0231 g) was placed in one leg of the apparatus. (DIPHOS)Mo(CO)$_4$[17] (0.0282 g, 0.0465 mmol) was added to the reference leg. CH_2Cl_2 was distilled into the apparatus, which was sealed under vacuum. Solvent levels equilibrated after 5 days at 25 °C, indicating the mole fractions of each solution were equivalent. The molecular weight of **4** was calculated to be 9706 ± 900.

(BISBI)Fe(CO)$_3$-CH$_2$Cl$_2$ (5). (Benzylideneacetone)tricarbonyliron (677 mg, 2.37 mmol) and 2,2'-bis((diphenylphosphino)methyl)-1,1'-biphenyl, BISBI[6] (1.304 g, 2.37 mmol), were stirred in 30 mL of toluene for 18 h. The solution was evaporated under vacuum, and the residue was chromatographed (silica gel, toluene) to give **5** (108 mg, 7%) as a yellow powder. X-ray-quality crystals were grown by diffusion of hexanes into a dichloromethane solution of **5**. Elemental analysis and X-ray crystallography indicated that **5** crystallized with one CH_2Cl_2 molecule of crystallization: ^1H NMR (CD_2Cl_2) δ 7.9-6.8 (m, 28 H), 4.28 (m, 4 H); $^{13}C\{^1H\}$ NMR (CD_2Cl_2) δ 215.1 (t, J_{PC} = 29 Hz, CO), 143.6 (1,1' C), 141.0 (virtual t, peak separation 20 Hz, ipso C_6H_5), 134.5 (virtual t, peak separation 18 Hz, 2,2' C), 134.2 (para C_6H_5), 132.0 (3,3' C), 131.7 (4,4' C), 130.8 (ortho C_6H_5), 128.6 (meta C_6H_5), 127.2 and 127.0 (6,6' C and 5,5' C), 35.3, (4-line AA'XX', J_{PC} = 28, $J_{PP'}$ = 100 Hz); $^{31}P\{^1H\}$ NMR (CD_2Cl_2) δ 72.6 (s); IR (CH_2Cl_2) 1970 (w), 1881 (s) cm^{-1}; HRMS calcd for M - 2CO ($C_{39}H_{32}P_2OFe$) 634.1277, found 634.1295. Anal. Calcd for $C_{42}H_{34}O_3Cl_2P_2Fe$: C, 65.56; H, 4.45; P, 8.97. Found: C, 65.63; H, 4.05; P. 8.55.

X-ray Crystallography. Diffraction data for both **3** and **5** were collected on a Nicolet P3f diffractometer. The 4371 measured data for **3** yielded 2304 independent, observed ($R > 6\sigma(F)$) data. A total of 6048 data were measured for **5**, producing 2847 independent, observed ($F > 4\sigma(F)$) data. Both structures were solved by direct methods and refined by full-matrix least-squares methods using the SHELXTL PLUS[18] software package. Details of the crystal data, experimental conditions, and a summary of refinement details are given in Table III and in the supplementary material. Atomic coordinates and isotropic displacement parameters for **3** and **5** are presented in Tables IV and V.

Acknowledgment. Financial support from the Office of Basic Energy Sciences, Department of Energy, is gratefuly acknowledged. We thank Texas Eastman Kodak for a generous gift of BISBI.

Supplementary Material Available: A full table of crystallographic data, figures with complete numbering schemes, and tables of bond lengths, bond angles, anisotropic thermal parameters, and hydrogen atom parameters (14 pages); observed and calculated structure factor amplitudes for **3** and **5** (30 pages). Ordering information is given on any current masthead page.

(16) Shriver, D. F.; Drezdzon, M. A. *The Manipulation of Air-Sensitive Compounds*; Wiley-Interscience: New York, 1986; p 177.
(17) Chatt, J.; Watson, H. R. *J. Chem. Soc.* **1961**, 4980.
(18) *SHELXTL PLUS*; Siemens Analytical X-ray Instruments, Inc.: Madison, WI 53719, 1989.

Contribution from the Departments of Chemistry, University of South Carolina, Columbia, South Carolina 29208, and State University of New York at Albany, Albany, New York 12222

Solid-State ^{95}Mo NMR Study of (Aryldiazenido)- and (Organohydrazido)polyoxomolybdates. Investigation of Model Compounds of Catalytic Molybdenum Environments

John C. Edwards,[†] Jon Zubieta,[‡] Shahid N. Shaikh,[‡] Quin Chen,[‡] Shelton Bank,[‡] and Paul D. Ellis*[,†]

Received November 7, 1989

The ^{95}Mo static powder and magic angle spinning NMR spectra of the central $\pm^1/_2$ transition of a number of (aryldiazenido)-polyoxomolybdates, (organohydrazido)polyoxomolybdates, and unsubstituted polyoxomolybdates were obtained. The spectra clearly demonstrated the existence of octahedral and tetrahedral sites within these compounds by the contrast between the respective line widths and the dependence under MAS conditions of the resonances from these sites. Variation of ligand coordination was also seen to yield a visible chemical shift to the octahedral molybdenum sites in selected complexes. An interactive graphics curve-fitting program was used to estimate the quadrupolar coupling constants, asymmetry parameters of the electric field gradients, the three principal elements of the shielding tensor, and the Euler angles relating the quadrupole and chemical shielding principal axis systems for the molybdenum sites from the static powder spectra. Assignments of the line shape components was made to the different molybdenum sites present in these species. The method of assignment, based on degree of distortion at the site, was vindicated by MO calculations carried out on a simple $[MoO_6]^{6-}$ model species. These MO calculations demonstrate the increase in the magnitude of the electric field gradient (and hence the value of A_{cc}) was one distorts the octahedral environment by a combination of bond length and angular variations. The effectiveness of the ^{95}Mo NMR technique to obtain these data from Mo(VI) compounds was thus demonstrated and has laid a foundation from which future solid-state ^{95}Mo NMR studies of biological and catalytic molybdenum systems can benefit by comparison of the results obtained with those obtained for these model compounds.

Introduction

The use of liquid-state ^{95}Mo NMR spectroscopy has developed into a very active area of research in the past 7 years and has been the subject of review by Minelli et al.[1] This rapid development is due to the importance of molybdenum in organometallic and inorganic chemistry[2] as well as bioinorganic chemistry.[3-8] Liquid-state ^{95}Mo NMR spectroscopy has been applied to studies of molybdates in impregnation solutions of catalysts[9,10] as well as to characterizing many Mo(VI) and Mo(IV) species that are believed to model the active sites of molybdenum enzymes such as xanthine oxidase, xanthine dehydrogenase, sulfite oxidase,

[†] University of South Carolina.
[‡] State University of New York at Albany.

(1) Minelli, M.; Enemark, J. H.; Brownlee, R. T. C.; O'Connor, M. J.; Wedd, A. G. *Coord. Chem. Rev.* **1985**, *68*, 169.
(2) Grieves, R. A.; Mason, J. *Polyhedron* **1986**, *5*, 415.
(3) Young, C. G.; Minelli, M.; Enemark, J. H; Miessler, G.; Janietz, N.; Kauermann, H.; Wachter, J. *Polyhedron* **1986**, *5*, 407.
(4) Bray, R. C.; Swann, J. C. *Struct. Bonding (Berlin)* **1972**, *11*, 107.
(5) Moura, J. J. G.; Xavier, A. V. In *New Trends in Bio-inorganic Chemistry*; Williams, R. J. P., Da Silva, J. R. R. F., Eds.; Academic Press: New York, 1978; Chapter 4, p 79.
(6) Spence, J. T. In *Metal Ions in Biological Systems*; Sigel, H., Ed.; Dekker: New York, 1975; Vol. 5, Chapter 6, p 279.
(7) Spence, J. T. *Coord. Chem. Rev.* **1983**, *48*, 59.

0020-1669/90/1329-3381$02.50/0

nitrogenase, and nitrogen reductase.[11-14] Only in a few previous instances have solid-state ^{95}Mo NMR studies of molybdates been reported,[15-17] in addition to one study of molybdenum hexacarbonyl adsorbed onto γ-alumina.[18] In general, the characterization of Mo(VI) species has become routine in the liquid state. In a recent study Bank et al.[19] studied the liquid-state ^{95}Mo NMR spectra of a select series of (aryldiazenido)- and (organohydrazido)-polyoxomolybdates in conjunction with several unsubstituted polyoxomolybdates. In their survey of the ^{95}Mo spectra obtained on this range of polyoxomolybdates, the resonances due to the mixed tetrahedral/octahedral molybdenum coordination, and the varying ligand coordination to molybdenum in these complexes, were easily identified on the chemical shift scale and by their respective line widths.

Recently, we have been interested in the characterization of molybdena on alumina hydrodesulfurization catalysts.[20,21] These catalysts, in their freshly prepared state, are thought to have mixed tetrahedral and octahedral molybdenum environments on the surface of the γ-alumina. With their mixed tetrahedral/octahedral environments, this range of (aryldiazenido)- and (organohydrazido)polyoxomolybdates can be seen to be excellent models of these catalytic systems. Also, the ligation of various nitrogen ligands to the molybdenum sites in these species will allow us to develop an understanding of the interaction of supported catalytic molybdenum sites with small organic molecules such as pyridine, which would be of interest in analysis of processes such as hydrodenitrogenation reactions. These compounds also represent primitive models of the active molybdenum sites in nitrogenases that are thought to have variably coordinated Mo(VI) nuclei at the active sites. The coordination of diazenido groups to Mo is an obvious model of the coordination of N_2 to the nitrogenase active site. The large framework surrounding the molybdenum atoms mimics the steric environment created by the protein in nitrogenase.

In this study we present the solid-state ^{95}Mo NMR spectra of the same range of polyoxomolybdates studied by Bank et al.[19] along with a range of related species in order to demonstrate the feasibility of the characterization of Mo(VI) complexes by solid-state NMR methods. One would expect the tetrahedral and octahedral environments to lead to variations in the quadrupolar coupling constant (Q_{cc}), which will manifest themselves in variations of the line widths of the respective resonances. Also, variations in the ligation will lead to chemical shift changes. The static powder spectra and the magic angle spinning (MAS) spectra are presented.

^{95}Mo is a quadrupolar nucleus of nuclear spin $I = {}^5/_2$ and a relatively high natural abundance (15.8%). It has a comparatively small quadrupole moment, Q, of 0.12×10^{-24} cm^2, which means that the line shapes in the solid-state are not too broad. Molybdenum has another NMR-active isotope, ^{97}Mo, which also has a nuclear spin $I = {}^5/_2$ and a similar magnetic moment but possesses a larger quadrupole moment ($Q = 1.1 \times 10^{-24}$ cm^2). This makes ^{97}Mo the least desirable choice, from a receptivity standpoint, as well as a simulation standpoint, when one wishes to observe the perturbation of the quadrupole line shape caused by the chemical shielding interaction.

Experimental Section

Materials. The synthesis and characterization of the compounds, $(Bu_4N)_2Mo_2O_7$ (**1**),[22] $[Bu_4N]_3[Mo_3O_8(OMe)(C_4O_4)_2]$ (**2**),[23] $[Bu_4N]_2[Mo_4O_{10}(OMe)_2(catecholate)_2]$ (**3**),[24] $[Bu_4N]_2[Mo_4O_{10}(OMe)_2(N_2PhMe)_2]$ (**4**),[19] $[Bu_4N]_2[Mo_4O_{10}(OMe)_2(N_2Ph_2)_2]$ (**5**),[19] $[Bu_4N]_2[Mo_4O_8(OMe)_2(NNC_6H_4\text{-}p\text{-}NO_2)_4]$ (**6**),[19] $[Bu_4N]_2[Mo_4O_{11}(OMe)(hydralazine)]$ (**7**),[19] $[Bu_4N]_2[Mo_6O_{19}]$ (**8**),[19] $[Bu_4N]_3[Mo_6O_{18}(NNC_6F_5)]$ (**9**),[19] $[Bu_4N]_3[Mo_5O_{16}(OMe)]$ (**10**),[23] $[Bu_4N]_4[Mo_4O_8(OMe)_2(C_4O_4)_4]\cdot MeOH$ (**11**),[25] $[Bu_4N]_2[Mo_2O_6(py\text{-}2\text{-}COO)_2]$ (**12**),[26] and $[Bu_4N]_2[Mo_8O_{16}(OMe)_6(N_2MePh)_6]$ (**13**),[19] were performed in the laboratory of J.Z. at the Chemistry Department, State University of New York at Albany, by the methods previously reported. In the text, the compounds will be referred to by the numbers assigned above.

NMR Spectroscopy. The solid-state, natural-abundance ^{95}Mo NMR spectra were obtained on a Varian XL-400 spectrometer operating in the so-called "side-line mode" at 26.06 MHz. Two probes were used in the static powder experiments—broad-band tunable 5-mm orthogonal powder and 7-mm MAS probes, both supplied by Doty Scientific Inc. (600 Clemson Rd., Columbia, SC 29223). The linear pulse amplifier used in the experiments was from ENI, Model LPI10. Typical power levels used were 576–625 W. The nonselective $\pi/2$ pulse was determined on a reference solution of 2 M Na_2MoO_4 at pH 11. In order to excite the central $\pm{}^1/_2$ transition, a selective pulse was used, which is obtained by dividing the nonselective pulse by a factor of $(I + {}^1/_2)$. In this case, the factor was 3. Typical values for the selective pulse, $(\pi/2)_s$, were between 1.4 and 1.9 μs for the 5-mm powder probe and between 2.8 and 3.1 μs for the 7-mm MAS probe. The selective pulse width values were checked by running a pulse width array on a solid standard sample (94.9% ^{95}Mo-enriched $(NH_4)_6Mo_7O_{24}\cdot 4H_2O$). In order to avoid the effects of acoustic ringing, a solid echo pulse sequence was used, which involves a selective $\pi/2$ preparative pulse followed by a selective π pulse,[27-30] the pulse sequence being

$$(\pi/2)_s\text{–}\tau_1\text{–}(\pi)_s\text{–}\tau_2\text{–acquire}$$

The FID is Fourier-transformed from the top of the resulting echo. A 16-step phase cycle was used to remove any artifacts due to imperfect pulses. Typical values for τ_1 and τ_2 were 60 and 55 μs, respectively. These echo delays can vary depending on the severeity of the ringing phenomenon. Relaxation delays used were on the order of 1 s although in some cases delays as long as 5–10 s were required. The majority of the MAS spectra were acquired by using the Doty 7-mm MAS probe with spinning speeds of between 3 and 4.8 kHz. The MAS spectra were obtained by using the same 16-step phase cycle solid echo pulse sequence, the only difference being that the τ_1 echo delay value was made equal to the reciprocal of the spinning speed.

In a recent note, Man and co-workers[31] alluded to a potential problem when utilizing selective pulses in quadrupolar systems. Namely, when one has a mixture of species with differing quadrupole coupling constants, one may have problems associated with the quantitative details of the experiment. This problem occurs when ω_Q (proportional to the quadrupole coupling constant) for some of the species is large compared to ω_{rf} while ω_Q for others is small relative to ω_{rf}. In this situation the rf pulse cannot be considered as selective. If one has mixed states, then the quantitation can be obtained by using a small slip angle excitation instead of selective $\pi/2$ pulses.[31] This situation is easy to diagnose with a nutation experiment.[32-40] We have performed such experiments on all of

(8) Bowden, F. L. In *Techniques and Topics in Bioinorganic Chemistry*; McAuliffe, C. A., Ed.; Macmillan Press: London, 1975; Part 3, p 205.
(9) Luthra, N. P.; Cheng, W.-C. *J. Catal.* **1987**, *107*, 154.
(10) Sarrazin, P.; Mouchel, B.; Kasztelan, S. *J. Phys. Chem.* **1989**, *93*, 904.
(11) Minelli, M.; Enemark, J. H.; Wieghardt, K.; Hahn, M. *Inorg. Chem.* **1983**, *22*, 3952.
(12) Buchanan, I.; Minelli, M.; Ashby, M. T.; King, T. J.; Enemark, J. H.; Garner, C. D. *Inorg. Chem.* **1984**, *23*, 495.
(13) Minelli, M.; Young, C. G.; Enemark, J. H. *Inorg. Chem.* **1985**, *24*, 1111.
(14) Young, C. G.; Enemark, J. H. *Inorg. Chem.* **1985**, *24*, 4416.
(15) Mastikhin, V. M.; Lapina, O. B.; Maximovskaya, R. I. *Chem. Phys. Lett.* **1988**, *148*, 413.
(16) Lynch, G. F.; Segel, S. L. *Can. J. Phys.* **1972**, *50*, 567.
(17) Kautt, W. D.; Krüger, H.; Lutz, O.; Maier, H.; Nolle, A. *Z. Naturforsch.* **1976**, *31a*, 351.
(18) Shirley, W. M. *Z. Phys. Chem.* **1987**, *152*, 41.
(19) Bank, S.; Liu, S.; Shaikh, S. N.; Sun, X.; Zubieta, J.; Ellis, P. D. *Inorg. Chem.* **1988**, *27*, 3535.
(20) Edwards, J. C.; Adams, R. D.; Ellis, P. D. *J. Am. Chem. Soc.*, in press.
(21) Edwards, J. C.; Ellis, P. D. Submitted for publication in *J. Am. Chem. Soc.*
(22) Day, V. W.; Friedrich, M. F.; Klemperer, W. G.; Shum, W. J. *J. Am. Chem. Soc.* **1977**, *99*, 6146.
(23) Chen, Q.; Ma, L.; Liu, S.; Zubieta, J. *J. Am. Chem. Soc.* **1989**, *111*, 5944.
(24) Kang, H.; Shaikh, S. N.; Nicholson, T.; Zubieta, J. *Inorg. Chem.* **1989**, *28*, 920.
(25) Chen, Q.; Liu, S.; Zubieta, J. *Inorg. Chim. Acta*, in press.
(26) Chen, Q.; .iu, S.; Zubieta, J. *Inorg. Chim. Acta* **1989**, *162*, 163.
(27) Solomon, I. *Phys. Rev.* **1958**, *110*, 61.
(28) Weisman, I. D.; Bennett, L. H. *Phys. Rev.* **1969**, *181*, 1341.
(29) Bonera, G.; Avogadro, A.; Borsa, F. *Phys. Rev.* **1968**, *165*, 171.
(30) Warren, W. W., Jr.; Norberg, R. E. *Phys. Rev.* **1967**, *154*, 277.
(31) Man, P. P.; Klinowski, J.; Trokiner, A.; Zanni, H.; Papon, P. *Chem. Phys. Lett.* **1988**, *151*, 143.
(32) Samoson, A.; Lippmaa, E. *J. Magn. Reson.* **1988**, *79*, 255.
(33) Yannoni, C. S.; Kendrick, R. D. *J. Chem. Phys.* **1981**, *74*, 747.
(34) Man, P. P.; Theveneau, H.; Papon, P. *J. Magn. Reson.* **1985**, *64*, 271.
(35) Hanssen, R.; Tijink, G. A. H.; Veeman, W. S. *J. Chem. Phys.* **1988**, *88*, 518.

our surface precursors and have found that all of the observable ^{95}Mo is in the limit where $\omega_Q \gg \omega_{rf}$. Hence, relative quantitative via the selective echo approach is a valid method.

A 30-MHz low-pass filter was used to remove any spurious signals from the rf transmitter generated by the XL-400 spectrometer. In a number of the spectra, spikes appear at chemical shifts of 1380 and −2458 ppm. They were caused by a loose connection between the inductors of the low-pass filter. The chemical shifts reported are with respect to the reference solution of 2 M Na_2MoO_4 at pH 11. The spectral width was 400 kHz in most cases. In general, no decoupling was used for the samples although decoupled spectra were obtained for $(NH_4)_6Mo_7O_{24}\cdot 4H_2O$ in order to determine the size of the dipolar interaction.

Line Shape Simulation. The static powder line shapes were simulated with an interactive graphical curve fitting (IGCF) program developed by Cheng et al.[41] The program has been used successfully to deconvolute quadrupolar central transition line shapes of salts with inequivalent crystal lattice sites. The program assumes that the chemical shielding and quadrupolar principal axis systems (PAS) are noncoincident. Using this program, one can extract the principal elements of the chemical shielding tensor, the quadrupolar coupling constant, assymmetry parameter of the electric field gradient, and the Euler angles relating the chemical shielding and quadrupole PAS frames.

In this program the Hamiltonian used to describe the system can be written as the sum of the Zeeman, quadrupolar, and shielding terms. The chemical shielding Hamiltonian has been transformed to the quadrupole PAS frame and expressed in terms of its value in the chemical shielding PAS frame. The total Hamiltonian for the system can be expressed as

$$H_{system} - H_Z = H_{CS} + H_Q$$

where

$$H_{CS} = \frac{\omega_0 I_Z \delta_{CS}}{2}\Bigg[(3\cos^2\theta - 1)\left(\frac{3\cos^2\beta - 1}{2} - (\eta_{CS}/2)\sin^2\beta\cos 2\gamma\right) + (\sin 2\theta\cos(\phi+\alpha))(-1.5\sin 2\beta - \eta_{CS}\sin\beta\cos\beta\cos 2\gamma) + (\sin 2\theta\sin(\phi+\alpha))(\eta_{CS}\sin\beta\sin 2\gamma) + (0.5\sin^2\theta\cos(\phi+\alpha))(3\sin^2\beta - (\eta_{CS}\cos 2\gamma)(1+\cos^2\beta)) + (0.5\sin^2\theta\sin 2(\phi+\alpha))(2\eta_{CS}\cos\beta\sin 2\gamma)\Bigg]$$

$$\delta_{CS} = \sigma_{33} - \sigma_0$$

$$\sigma_0 = (1/3)(\sigma_{11} + \sigma_{22} + \sigma_{33})$$

$$\eta_{CS} = (\sigma_{11} - \sigma_{22})/\delta_{CS}$$

$$H_Q(\pm_1/_2) = -(R/6\omega_0)[A(\phi)\cos^4\theta + B(\phi)\cos^2\theta + C(\phi)]$$

$$R = \omega_q^2[I(I+1) - 3/4]$$

$$A(\phi) = (-27/8) - (9/4)\eta_Q\cos 2\phi - (3/8)\eta_Q^2\cos^2 2\phi$$

$$B(\phi) = (30/8) - (\eta_Q^2/2) + 2\eta_Q\cos 2\phi + (3/4)\eta_Q^2\cos^2 2\phi$$

$$C(\phi) = (-3/8) + (\eta_Q^2/3) + (\eta_Q/4)\cos 2\phi - (3/8)\eta_Q^2\cos^2 2\phi$$

$$\omega_q = 3e^2qQ/2I(2I-1)h = 3Q_{cc}/2I(2I-1)h$$

$$\eta_Q = (V_{11} - V_{22})/V_{33}$$

$$q = (1/e)V_{33}$$

The values V_{11}, V_{22}, and V_{33} are the three principal elements of the electric field gradient (EFG) tensor and σ_{11}, σ_{22}, and σ_{33} are the three principal values of the shielding tensor. The resonance frequency is denoted by ω_0. The values η_Q and η_{CS} are the asymmetry parameters of the EFG and the chemical shielding tensor, respectively. The angular values ϕ and θ are the Euler angles relating the magnetic field H_0 to the PAS frame of the quadrupole tensor, and α, β, and γ are the Euler angles which relate the chemical shielding and quadrupole PAS frames.

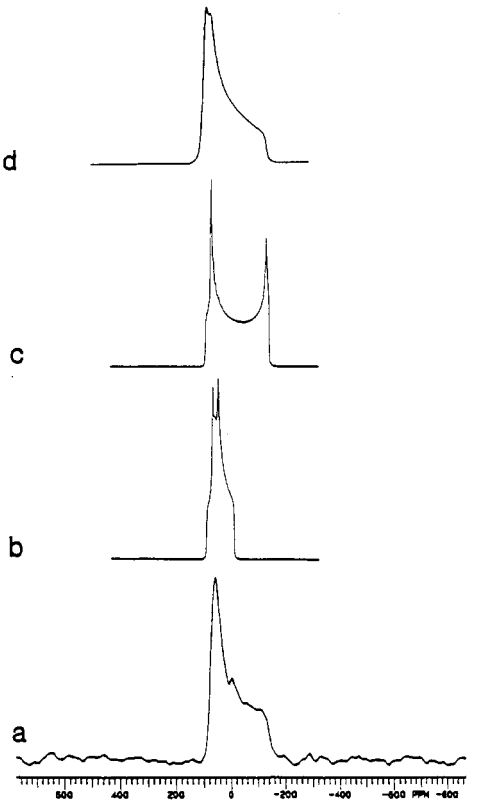

Figure 1. Static powder spectrum and simulated spectra of $(Bu_4N)_2Mo_2O_7$ (**1**): (a) static powder spectrum, obtained with cross polarization and high-power decoupling, 20-ms contact time, 3477 transients, and 5-s recycle delay; (b) simulated spectrum using quadrupole parameters only; (c) quadrupole and chemical shielding tensor components with coincident PAS frames; (d) quadrupole and chemical shielding tensor components with noncoincident PAS frames.

The program uses a seven-parameter (Q_{cc}, η_Q, δ_{CS}, η_{CS}, α, β, γ) variable-size simplex algorithm, which is in fact a simplex within a simplex. The various quadrupole and shielding parameters are simplexed, and for each simplex step the line shape is calculated. The line shape or line shape components are then simplexed by varying the scale and offset of the simulated line shape until the best fit is obtained. The program does not contain any scaling parameters based on the expected relative intensities of the component line shapes; it simply scales the various components in order to obtain the "best fit". Thus, for example, if one of the components had a longer T_1 than the other and the relaxation delay used in the NMR experiment was less than $5T_1$ for that component, the relative intensities of the line shapes would not be a true representation of the ratios of the number of molybdenum atoms present in the various inequivalent sites. This is indeed the case in several of the spectra that we have obtained, as will be seen later.

In order to demonstrate the necessity of using a seven-parameter fitting procedure, we present, in Figure 1, a series of spectra that shows the sensitivity of the ^{95}Mo line shape of $(Bu_4N)_2Mo_2O_7$ (**1**) to the various fitting parameters. Species **1** consists of two oxygen-bridged tetrahedral molybdates[22] and posesses rigorous C_2 symmetry. Crystallographically and chemically there is only one molybdenum site. The static powder line shape (Figure 1a), however, seems on first inspection to indicate the presence of more than one resonance. Figure 1b shows the simulated "best fit" using only the quadrupolar parameters (a two-parameter fit: Q_{cc} and η_Q). Obviously, this is not a good fit and Figure 1c shows the improvement of the fit when the chemical shift parameters are also introduced (a four-parameter fit: Q_{cc}, η_Q, δ_{CS}, η_{CS}). This fit represents the so-called "Baugher fit", which assumes the coincidence of the quadrupole and chemical shielding tensor PAS frames.[42] An adequate fit is finally obtained when one incorporates the three Euler angles (Figure 1d) that relate the noncoincident PAS frames (a seven-parameter fit). For the parameter values obtained see Table II. In this case the line shape

(36) Geurts, F. M. M.; Kentgens, A. P. M.; Veeman, W. S. *Chem. Phys. Lett.* **1985**, *120*, 206.
(37) Samoson, A.; Lippmaa, E. *Chem. Phys. Lett.* **1983**, *100*, 205.
(38) Samoson, A.; Lippmaa, E. *Phys. Rev. B* **1983**, *28*, 6567.
(39) Kentgens, A. P. M.; Lemmens, J. J. M.; Geurts, F. M. M.; Veeman, W. S. *J. Magn. Reson.* **1987**, *71*, 62.
(40) Trokiner, A.; Man, P. P.; Thèveneau, H.; Papon, P. *Solid State Commun.* **1985**, *55*, 929.
(41) Cheng, J. T.; Edwards, J. C.; Ellis, P. D. *J. Phys. Chem.* **1990**, *94*, 553.
(42) Baugher, J. F.; Taylor, P. C.; Oja, T.; Bray, P. J. *J. Chem. Phys.* **1969**, *11*, 4914.

can only be described by a simulated line shape involving a seven-parameter fit. It is important to note that the fit, albeit with seven parameters, is constrained; i.e., we know the exact functional form of the line shape. However, difficulties arise when one has a line shape that arises from multiple sites within a species and/or multiple species. It may seem that one is performing a free-floating 14- or 21-parameter fit. This is not the case. One knows from the outset the number of inequivalent molybdenum sites present in the species, and the parameters for each component are constrained. The signal to noise levels of many of the spectra only allowed an evaluation of the quadrupole parameters (Q_{cc} and η_Q), while others allowed only an evaluation of the quadrupole and chemical shielding parameters, without the Euler angles being found. It must be stressed here that even with excellent signal to noise levels, one also has to be concerned with the line shape itself. That is, the relative magnitudes of the quadrupole and chemical shielding interactions must be manifested in the line shape! It is our opinion that whenever one can obtain spectra with a high enough signal to noise ratio, this general approach of assuming noncoincidence of the PAS frames is the only way of obtaining the correct parameter values. There is, however, a potential for the values obtained to have large errors associated with them, especially in the case of the chemical shift anisotropy values. This arises in cases when the chemical shielding effects on the line shape are small.

In previous work on ^{87}Rb, we have tried to evaluate the error involved in this process.[41] We have met with only limited success in this respect, although we estimated the errors (for the ^{87}Rb salts) to be the following: Q_{cc}, ±0.1 MHz; η_Q, ±0.04; η_{CS}, ±0.04; α and γ, ±4°; β ± 1°. Of course, these errors will be larger if the signal to noise ratio is not adequate—this may be the case with the errors involved in the simulation of some of the spectra obtained in the present work. It is planned to compare the data that we have obtained on the ^{87}Rb salts with ^{87}Rb single-crystal NMR data. We will also perform a thorough statistical least-squares analysis on the powder line shape tensor values that are obtained when the simulation is treated as a two-, four-, seven-, or fourteen-parameter fit. This should accurately give us the quadrupole and chemical shielding parameters and the relative errors involved in this fitting procedure.

The program becomes increasingly insensitive to changes in the shielding parameters in cases where large quadrupolar interactions are present, i.e. Q_{cc} > 5–6 MHz. In these cases the errors in the obtained shielding parameters have the potential for being larger than those observed in lower Q_{cc} line shapes. Thus, in these cases only the quadrupole parameters were obtained, as the chemical shift interaction does not manifest itself in the line shape.

Results

A summary of the chemical shift and line width (full width at half-height) data is presented in Table I along with the data obtained in a previous study of molybdenum in catalytic environments.[20] In the case of the static spectra, the chemical shift data correspond to positions of singularities and in the case of MAS spectra to peak maxima and should not be interpreted as components of the chemical shielding interaction. The calculated quadrupole and chemical shielding parameters obtained from the line shape simulation program are displayed in Table II. It should be noted that in many cases certain parameters, such as shielding tensor components or Euler angles, are represented with a postscript label. This indicates that a significant improvement of the fit could not be obtained by introducing those particular parameters into the fitting procedure.

Discussion

Theoretical Background. One of the main motivations for performing this investigation was the fact that many of the complexes had been thoroughly studied in the liquid state[19] and chemical shift data were available on the species as well as interesting inferences as to the quadrupolar coupling constants of the different sites in these complexes. In many cases there are mixed octahedral and tetrahedral sites in the same complex. The difference in Q_{cc} among tetrahedral (high symmetry), distorted tetrahedral, and octahedral (lower symmetry due to distortion) allows one to distinguish between the two sites in a solid-state ^{95}Mo NMR spectrum especially under conditions of magic angle rotation. The reason that the octahedral polyoxomolybdates tend to have distorted molybdenum environments is due to the varying coordination number of the oxygen atoms on these compounds. The oxygen atoms can be coordinated to between one and four molybdenum atoms, leading to a large variation in Mo–O bond lengths (1.70–2.3 Å) and thus to distorted environments.

Table I. ^{95}Mo Chemical Shift and Line Width Data of the Static Powder Spectra for the Molybdenum Complexes Studied

compd	singularity and peak positions, ppm[a] static	singularity and peak positions, ppm[a] MAS[b]	line width,[c] kHz static	line width,[c] kHz MAS	Figure
$[Bu_4N]_2Mo_2O_7$	49.5 3 −127.5	−6.5 (4700)	1.66	0.06	1a,c
$[Bu_4N]_3$-$[Mo_3O_8(OMe)$-$(C_4O_4)_2]$	202 −285 −53	228 81.5 −183 −317.5 (3800)	20.24	20.24	3a,b
$[Bu_4N]_2$-$[Mo_4O_{10}(OMe)_2$-$(catecholate)_2]$	664 212.5 −307	590.5 461.5 221 88 −40.5 −105.5 −275 −370 (3320)	30.72	20.42	4a,b
$[Cu_4N]_2$-$[Mo_4O_{10}(OMe)_2$-$(N_2MePh)_2]$	−43.5	−47 (4150)	12.03	1.70 30.92	5a,b
$[Bu_4N]_2$-$[Mo_4O_{10}(OMe)_2$-$(N_2Ph_2)_2]$	977 450 −14 −400	−30.5 (4300)	8.03	0.75 29.03	6a,b
$[Bu_4N]_2$-$[Mo_4O_8(OMe)_2$-$(N_2Ph$-p-$NO_2)_4]$	960 70 −56	−46 (4470)	9.64	3.40	7a,b
$[Bu_4N]_2$-$[Mo_4O_{12}$-(hydralazine)]	31	270 −7 −213 (4360)	9.93	2.90	8a,b
$[Bu_4N]_2Mo_6O_{19}$	505 −395	446 327 288.5 421.5 (3400)	28.80	28.70	9a,b
$[Bu_4N]_3[Mo_6$-$O_{18}(NNC_6F_5)]$	58.5		8.28		10
$[Bu_4N]_3$-$[Mo_5O_{16}(OMe)]$	706 270 5 −490 −1380	53.5 (4515)	7.53	13.73	11a,b
$[Bu_4N]_4[Mo_4O_8$-$(OMe)_2(C_4O_4)_4]\cdot$ MeOH	1343 939 145 −382		53.60		12
$[Bu_4N]_2[Mo_2O_6$-$(C_5H_4N$-2-$COO)_2]$	96.5 −171	−53.5 (4280)	12.63	4.32	13a,b
$[Bu_4N]_2$-$[Mo_8O_{16}(OMe)_6$-$(N_2MePh)_6]$	652 136 −57.5 −510.5	227 −13.5 (4125)	21.70	18.60	14a,b

[a] Shifts correspond to the relative peak maxima (MAS spectra) and singularities (static spectra) observed in the spectra. [b] The MAS spin speed (in Hz) is displayed in parentheses below the MAS shift values; singularitity and peak positions are reported to the nearest 0.5 ppm. [c] Full width at half-height.

In our arguments (to be outlined below) we have based our tentative assignments of the different molybdenum sites upon the assumed relationship between the degree of distortion at the molybdenum site and the Q_{cc} values obtained for the components of the line shape. By distortion, we are referring to any bond length or angular deviations from pure octahedral molecular symmetry, i.e. deviation of single Mo–O bond from some minimum energy bond length, angular deviation of the O–Mo–O bond angles from 90°, or any combination of the two. We will argue that the Q_{cc} values increase as the degree of distortion of the molybdenum environment increases. We have investigated the integrity of this

Table II. Parameters Obtained from Simulation of Various Model Compounds

complex[a]	Q_{cc}, MHz	η_Q	σ_{11}, ppm	σ_{22}, ppm	σ_{33}, ppm	α, deg	β, deg	γ, deg
$Na_2MoO_4 \cdot 2H_2O$[b]	~1.00	0.00	*c*	*c*	*c*	*c*	*c*	*c*
$PbMoO_4$[b]	2.05	0.20	−109	9	12	43	10	−56
$(NH_4)_2Mo_2O_7$[b]								
tet	2.44	0.47	−35	15	51	4	79	41
oct	3.41	0.07	−54	−7	12	*c*	*c*	*c*
$(NH_4)_6Mo_7O_{24} \cdot 4H_2O$[b]								
type I	2.98	0.73	*c*	*c*	*c*	*c*	*c*	*c*
type II	5.76	0.42	*c*	*c*	*c*	*c*	*c*	*c*
type III	3.73	1.00	*c*	*c*	*c*	*c*	*c*	*c*
MoO_3[b]	3.49	0.99	18	178	349	63	70	−89
$Mo_8O_{26}^{4-}$[b]								
tet	0.34	0.00	−35	−35	10	*c*	*c*	*c*
oct	6.12	0.53	*c*	*c*	*c*	*c*	*c*	*c*
$[Bu_4N]_2Mo_2O_7$	1.14	0.75	−7	19	204	−33	−5	54
$[Mo_6O_{19}]^{2-}$	4.90	0.05	35	426	445	77	0	49
$[Mo_3O_8(OMe)(C_4O_4)_2]^{3-}$	3.82	0.40	23	25	54	40	12	40
	4.26	0.95	−81	60	221	1	−8	−64
$[Mo_4O_{10}(OMe)_2(Cat)_2]^{2-}$								
oct 1	6.00	0.95	*c*	*c*	*c*	*c*	*c*	*c*
oct 2	6.76	0.05	*c*	*c*	*c*	*c*	*c*	*c*
$[Mo_4O_{10}(OMe)_2(N_2MePh)_2]^{2-}$								
tet	2.79	0.46	−17	10	35	*c*	*c*	*c*
oct	4.61	0.10	*c*	*c*	*c*	*c*	*c*	*c*
$[Mo_4O_{10}(OMe)_2(N_2Ph_2)_2]^{2-}$								
tet	2.30	0.20	−40	−12	16	*c*	*c*	*c*
oct	5.16	0.16	−63	52	80	*c*	*c*	*c*
$[Mo_4O_8(OMe)_2(N_2Ph\text{-}p\text{-}NO_2)_4]^{2-}$								
tet	2.51	0.16	*c*	*c*	*c*	*c*	*c*	*c*
oct	4.90	0.19	*c*	*c*	*c*	*c*	*c*	*c*
$Mo_5O_{16}(OMe)^{3-}$								
tet	2.17	0.07	*c*	*c*	*c*	*c*	*c*	*c*
oct	5.52	0.80	*c*	*c*	*c*	*c*	*c*	*c*
oct	5.46	0.32	*c*	*c*	*c*	*c*	*c*	*c*
$[Mo_2O_6(py\text{-}2\text{-}COO)_2]^{2-}$	3.20	0.64	−139	173	175	34	28	−28

[a] py = pyridine; Cat = catecholate. [b] See ref 20. [c] These values were not used in the curve-fitting process, as their addition as parametres did not markedly improve the fit that was obtained.

assumption by performing some molecular orbital calculations[43] on the effect of molecular distortion on the value of the molybdenum Q_{cc}.

In these molecular orbital calculations we used the Gaussian 86[43] STO-3G calculation to obtain the three principal components of the EFG tensor (q_{ii}) for the $[MoO_6]^{6-}$ model anion. Figure 2 shows the results of these calculations. Figure 2a shows the plot of Q_{cc} versus bond length variation along the hypothetical z axis of the octahedron. It should be noted that the bond lengths of the pure octahedron were made to be 2.1 Å. Compression of the z-axis bonds can be seen to cause an increase in the value of Q_{cc}, while elongation results in a less dramatic increase in $|Q_{cc}|$ in which the sign of Q_{cc} is changed to a negative value. Figure 2b shows the plot Q_{cc} against angular variation of the xy-plane Mo–O bonds first where all the bonds are 2.1 Å and second when the z-axis bonds are elongated to 2.3 Å. Again, the trend of increased $|Q_{cc}|$ with increased angular deviation is demonstrated in both cases. It should be noted that the effect is greatly reduced when the angles are varied when the z-axis bonds are elongated to 2.3 Å. It should be noted that the MO calculation overestimates the size of the electric field gradient. However, the overall trends reveal the information that we are looking for.

We have also investigated the effect of ligand variation on the value of Q_{cc} by performing the same calculations on the same octahedral model compound by substituting S^{2-} ligands for the O^{2-} ligands. The results obtained are as follows: $[MoO_5S]^{6-}$, Q_{cc} = −14.039 MHz; $[MoO_4S_2]^{6-}$ (trans S), Q_{cc} = −22.99 MHz; $[MoO_4S_2]^{6-}$ (cis S), Q_{cc} = 13.50 MHz. These results demonstrate the general trend of Q_{cc} increase with ligand substitution although the relationship between the symmetry of the substitutions and the size of Q_{cc} is not demonstrated.

A discussion of the effect of these distortions on the molecular orbitals and their corresponding impact upon the EFG tensor will be given in the Appendix. A more thorough analysis of these and other molecular orbital calculation results will be presented in a future publication.[44]

Experimental Background. We have investigated several tetrahedral and octahedral molybdenum species in the light of their being model systems of molybdenum species present in hydrodesulfurization catalysts.[20] The pure tetrahedral symmetry species investigated was $Na_2MoO_4 \cdot 2H_2O$, and it appeared to have a very small quadrupole coupling constant, yielding a 3.26-kHz line width in the static spectrum, which narrowed to 340 Hz in the 2.9-kHz MAS spectrum. Two distorted tetrahedral species, $PbMoO_4$ and $Al_2(MoO_4)_3$, were investigated, and they yielded larger Q_{cc} values (2–3 MHz). Purely octahedral species were also investigated, and they showed a range of Q_{cc} values and varied considerably in their line widths depending upon the distortion present in the octahedral structures. Depending upon the value of the Q_{cc} (related to the degree of distortion in the octahedral structure), the resonances would narrow by a high degree in the case of small Q_{cc} or by a small degree in the case of large Q_{cc} upon magic-angle spinning. Octahedral species investigated include $(NH_4)_6Mo_7O_{24} \cdot 4H_2O$, MoO_3, $[Bu_4N]_2Mo_6O_{19}$, and $H_3PMo_{12}O_{40}$. Mixed octahedral/tetrahedral species that were investigated were $(NH_4)_2Mo_2O_7$ and $[Bu_4N]_4Mo_8O_{26}$. Both sample spectra demonstrated the presence of the two sites by the obvious presence of a narrow, small Q_{cc} resonance superimposed on a broader, high-Q_{cc} line shape. The presence of the two resonances was accentuated by the MAS experiments, which caused a greater narrowing of the tetrahedral resonance, thus highlighting its presence. The spectra of these species are shown in a submitted publication by Edwards et al.[20]

(43) Frish, M. J.; Brinkley, J. S.; Schlegel, H. B.; Raghavachari, K.; Melius, C. F.; Martin, R. L.; Stewart, J. J. P.; Bobrowicz, F. W.; Rohlfing, C. M.; Kahn, L. R.; Defrees, D. J.; Seeger, R.; Whiteside, R. A.; Fox, D. J.; Fleuder, E. M.; Pople, J. A. *Gaussian 86*; Carnegie-Mellon Quantum Chemistry Publishing Unit: Pittsburgh, PA, 1984.

(44) Edwards, J. C.; Ellis, P. D. Unpublished results to be submitted for publication.

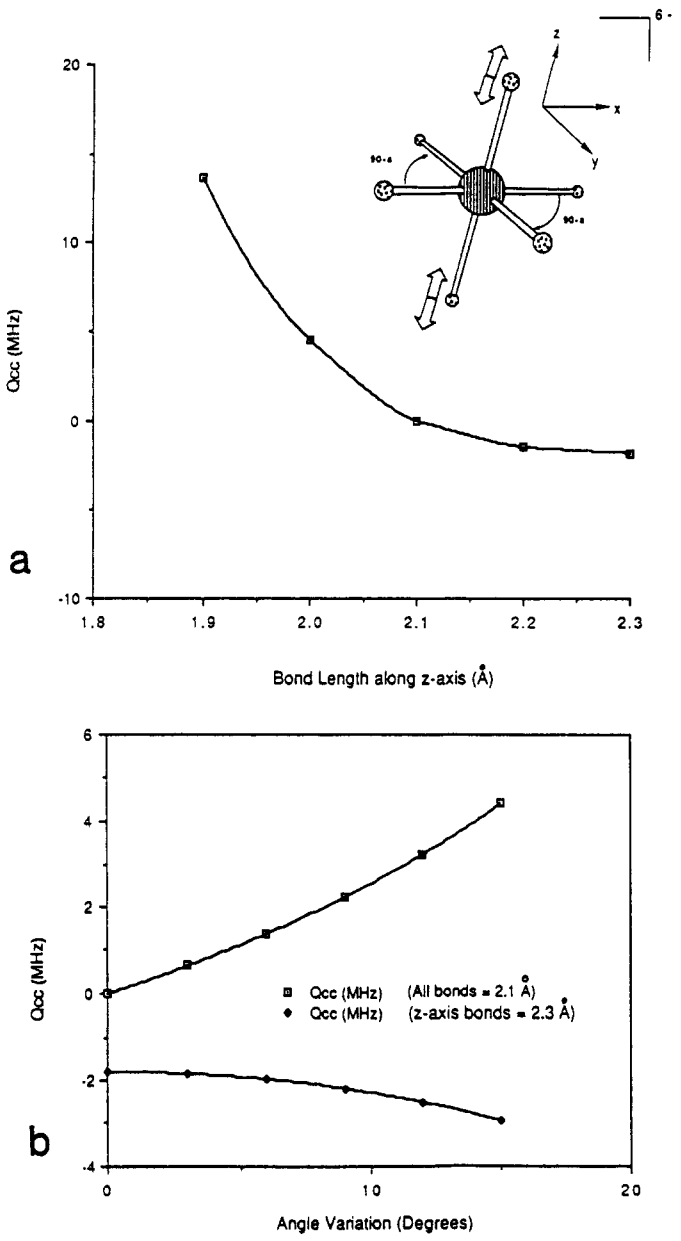

Figure 2. Results of Gaussian 86 STO-3G calculation: Plots of the calculated value of Q_{cc} against (a) bond length variation (from 2.1 Å) and (b) angular variation (from 90°), (i) when all bonds = 2.1 Å and (ii) when z-axis bonds are elongated to 2.3 Å, for the octahedral model species $[MoO_6]^{6-}$.

These results serve as background to the present investigation.

Present Investigation. In this publication we will expand upon the investigation of these octahedral and mixed tetrahedral/octahedral species to include a range of (aryldiazenido)- and (organohydrazido)polyoxomolybdates. Figure 3 shows the static, MAS, and simulated spectra of a purely octahedral molybdenum species $[Bu_4N]_3[Mo_3O_8(OMe)(C_4O_4)_2]$[23] (**2**). Species **2** contains three octahedra in which a bridging methoxide ligand is common to all three octhedra. Two of the octahedra have bridging oxygen atoms, two terminally bound oxygen atoms, and an oxygen atom shared with a bridging squaric acid ligand, while the remaining octahedron has only one terminally bound oxygen atom and two oxygen atoms shared with two squaric acid ligands. The species has a rhombohedral space group $R3c$, with 18 molecules per unit cell. This complex displays a two-component, second-order quadrupole static powder line shape, which can be approximated by the IGCF program. The simulated parameters of the two components are shown in Table II, and the simulated line shapes are shown in Figure 3c. The MAS spectrum (Figure 3b) illustrates that line shapes of species with large Q_{cc} values, under magic angle spinning conditions, are not affected in such a way that they

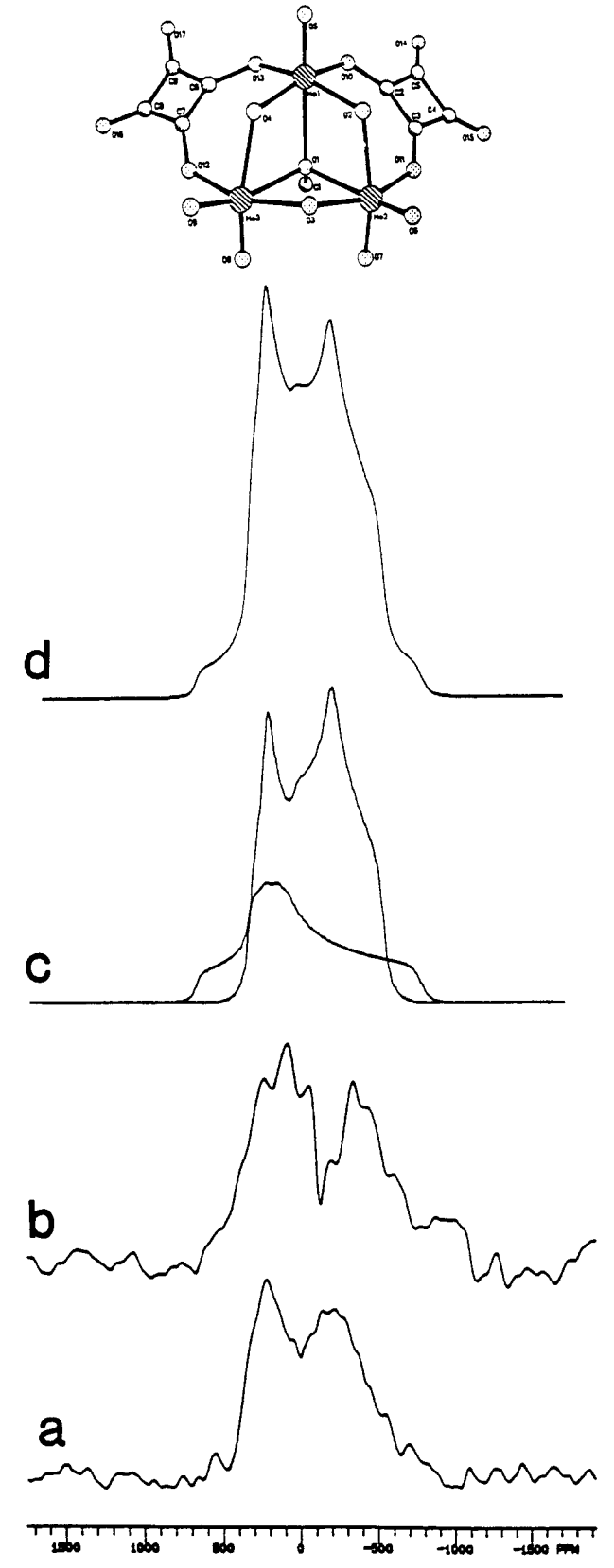

Figure 3. Static powder, MAS, and simulated spectra of the central $\pm^1/_2$ transition of a purely octahedral species: (a) static powder spectrum of species **2**, $[Bu_4N]_3[Mo_3O_8(OMe)(C_4O_4)_2]$, 207 100 transients, 0.5-s recycle delay, LB = 1500 Hz; (b) corresponding 3.8-kHz MAS spectrum, 142 324 transients, 0.5-s recycle delay, LB = 2000 Hz; (c) simulated spectrum obtained from the IGCF program; (d) deconvolution of the two contributions to the line shape. Note: The simulated spectra are not on the same scale as the experimental.

undergo dramatic narrowing, as is the case with tetrahedral species with low Q_{cc} values. However, in this particular case a large number of spinning sidebands have added to the number of discontinuities present in the spectrum, indicating the presence of a chemical shielding interaction. Our simulation of the line shape revealed the presence of a considerable chemical shift anisotropy (CSA) in this species. In order for us to make an assignment of the two tensors with the two sites in the molecule, we must determine which site has the more distorted environment, which would lead to a larger value of Q_{cc}. The sites with two terminally bound oxygen atoms have a greater degree of freedom than the site with only one terminal oxygen atom and thus will tend to have a less distorted environment because the terminal bonds can compensate for distortion and maintain a more closely octahedral environment. This argument demonstrates itself, modestly in this particular case, in the relative angular deviation from 90° observed for the two types of site found in this molecule—9.6° for the single terminal bond site and 9.5° for the double terminal bond sites. On the basis of this fact, we can tentatively assign the two sites with the higher degree of freedom (which leads to lower distortion) to the larger component with a Q_{cc} of 3.82 MHz, while the other site is responsible for the smaller component with a Q_{cc} of 4.26 MHz. The small difference in the Q_{cc} values also reflects the small difference in the angular deviations of the two sites. This assignment is also reinforced by the fact that the relative intensities of the two components, deconvoluted by our simulated, are very different, with the smaller Q_{cc} component being the more intense by about a factor of 2. This is in agreement with the ratio of the two sites with respect to each other. It is important, however, to use the intensity data with caution. In this particular case, the relative ratios of the areas under the line shapes are in agreement with the ratio of the number of molybdenum atoms in each site. This indicates that the relaxation delay used was greater than $5T_1$ for both of the molybdenum types. This will not always be the case, as we will see later. The assignment is also reinforced by an angular distribution study of a structurally similar molecule (species **10**), which will be discussed later.

Shown in Figure 4 is another example of a structurally complex system containing only octahedral molybdenum centers. This complex, **3**, consists of four octahedra in two different distorted environments[24]—the structure is shown in Figure 4. The static spectrum (Figure 4a) demonstrates the existence of more than one resonance. The deconvolution of these two contributions, apparently due to the two different octahedral environments, is shown in Figure 4d, while the simulated spectrum is shown in Figure 4c. The small amount of narrowing upon magic angle spinning at 3.3 kHz is again indicative of octahedral species with moderately large values of Q_{cc}. The simulation was carried out by assuming that the two line shapes were purely quadrupolar, with no contribution from a chemical shift anisotropy. One is a high EFG asymmetry line shape (η_Q = 0.95) with Q_{cc} = 6.00 MHz. As both sites have a similar degree of distortion in their octahedral environments, they possess similar values of Q_{cc}. In suggesting an assignment as to which tensor relates to which site, we will again base our argument on the apparent relationship between the Q_{cc} and the degree of distortion that is present at the two different sites. Inspection of the crystallographic data reveals that the catecholate-coordinated molybdenum possesses an average angular deviation of 9.6° from the expected 90° octahedral angle, while the methoxide-coordinated molybdenum sites possess a 10.2° average deviation. On the basis of these deviations, we can assign the smaller Q_{cc} (6 MHz and η_Q = 0.95) to the catecholate-coordinated molybdenum sites and the larger Q_{cc} (6.76 MHz and η_Q = 0.05) to the remaining two molybdenum sites. Such a conclusion is consistent with our calculations summarized in Figure 2. As will be seen later, the assignment of the component with the low η_Q value is consistent with the values of η_Q obtained for similarly structured species containing methoxide-coordinated, octahedral molybdenum sites, namely species **4**–**6**. The high η_Q value obtained for the catecholate-coordinated sites is also in agreement with the lack of symmetry operations associated with this site.

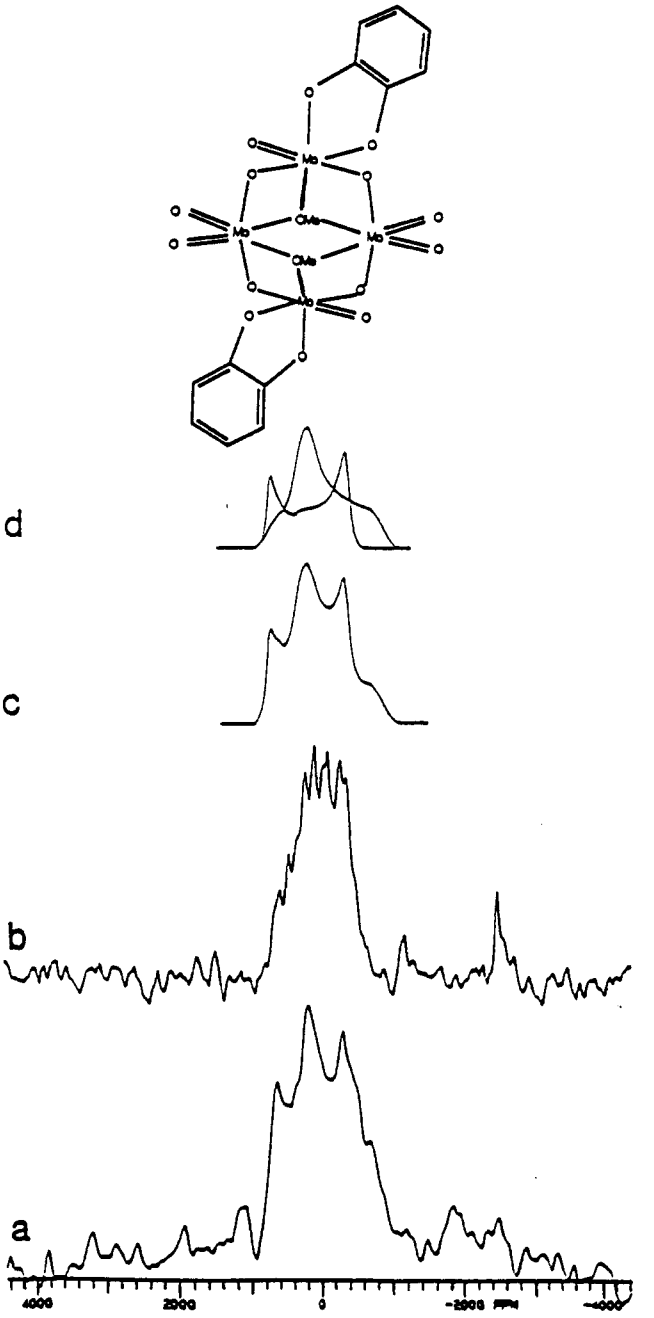

Figure 4. Static powder, MAS, and simulated spectra of a purely octahedral (organohydrazido)molybdate: (a) static powder spectrum of $[Bu_4N]_2[Mo_4O_{10}(OMe)_2(Cat)_2]$ (**3**), 209 806 transients, 0.5-s recycle delay, LB = 3000 Hz; (b) corresponding 3.1-kHz MAS spectrm, 139 500 transients, 0.5-s recycle delay; (c) simulated spectrum obtained from the IGCF program; (d) deconvolution of the two contributions to the line shape. Note: The simulated spectra are not on the same scale as the experimental.

We will now look at the results obtained from the (organohydrazido)- and (aryldiazenido)polyoxomolybdates that contain tetrahedral/octahedral sites. Figure 5 shows the static powder (Figure 5a) and 4-kHz MAS (Figure 5b) spectrum of the (organohydrazido)molybdate, species **4**. The structure of this compound consists of a methoxy-bridged binuclear core $[MoO(NNMePh)(\mu\text{-}OCH_3)_2MoO(NNMePh)]^{2+}$ bridged by two double bridging bidentate $[MoO_4]^{2-}$ units.[45] The two tetrahedral sites are equivalent, as are the two octahedral sites. The static powder spectrum illustrates the presence of more than one molybdenum site, while the 4.15-kHz MAS spectrum makes the distinction even more obvious. The narrow peak is due to the high-symmetry bridging $[MoO_4]$ sites, while the broader resonance is due to the

(45) Shaikh, S. N.; Zubieta, J. *Inorg. Chem.* **1988**, *27*, 1896.

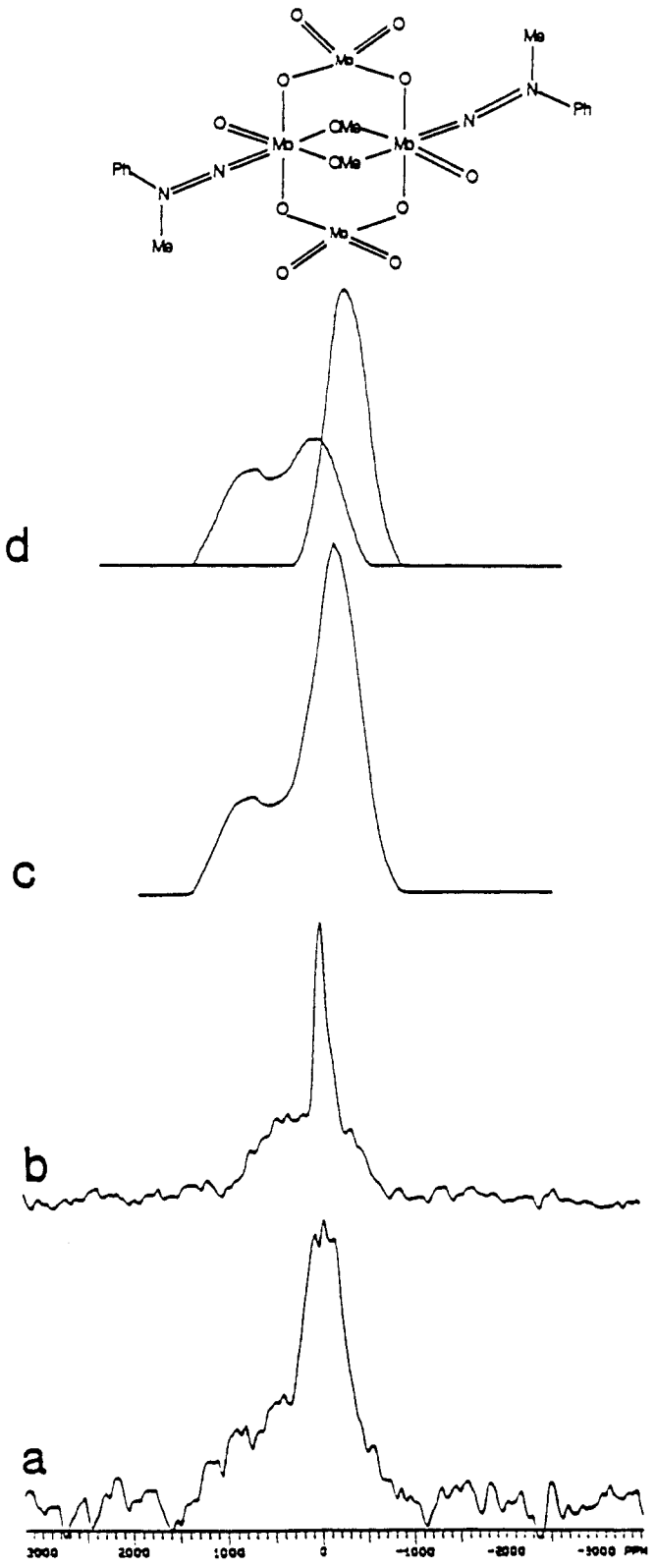

Figure 5. Static powder, MAS, and simulated spectra of the central $\pm^1/_2$ transition of a mixed tetrahedral/octahedral molybdenum site species, $[Bu_4N]_2[Mo_4O_{10}(OMe)_2(N_2PhMe)_2]$ (**4**): (a) static powder spectrum, 14 241 transients, 4-s recycle delay, LB = 3000 Hz; (b) corresponding 4-kHz MAS spectrum, 31 500 transients, 2-s recycle delay, LB = 3000 Hz; (c) simulated spectrum; (d) deconvolution of the two contributions to the line shape. Note: The simulated spectra are not on the same scale as the experimental.

octahedral sites. There is a slight shift to lower shielding of the octahedral resonance, which is due to the coordination of nitrogen to these sites. Figure 5c shows the simulated spectrum, while Figure 5d shows the deconvolution of the two contributions to the line shape. The narrower, more intense peak appearing at −43 ppm is due to the tetrahedral contribution showing a sizable Q_{cc} of 2.79 MHz, a medium-sized η_Q value of 0.46, and a small chemical shielding anisotropy (see Table II). The broad octahedral peak is due to a Q_{cc} of 4.61 MHz and an η_Q value of 0.10. As was mentioned previously, the low value of η_Q obtained for the octahedral site is consistent with the η_Q value obtained for species **3**. In this particular case, the inclusion of a chemical shielding interaction at the octahedral sites did not improve the "best fit" conditions described previously. It should be noted that the ratio of the areas of the two contributions is about 1:1, as would be expected.

Another mixed-site (organohydrazido)molybdate is species **5**, which has a structure similar to that of the previously described molybdate, except with two phenyl groups rather than a phenyl and a methyl group attached to the coordinated hydrazine.[46] It has been found that the two tetrahedral sites as well as the two octahedral sites are NMR equivalent. The static powder spectrum (Figure 6a) again demonstrates the presence of the tetrahedral and octahedral sites, while the 4.3-kHz MAS spectrum (Figure 6b) accentuates the different resonances owing to the considerable narrowing of the line due to the bridging $[MoO_4]$ group. Figure 6c shows the simulated spectrum of this compound, while Figure 6d showed the deconvolution of the two contributions to the line shape. The intense tetrahedral molybdenum line shape is due to a Q_{cc} of 2.30 MHz, $\eta_Q = 0.20$. The relatively large value of Q_{cc} is indicative of the distorted nature of the tetrahedral sites in these species, with the corresponding average angular deviation from 109.5° being 2.5°. The broader octahedral resonance is chemically shifted to lower shielding due to the coordination of nitrogen to the molybdenum and corresponds to an estimated Q_{cc} of 5.16 MHz, $\eta_Q = 0.16$, with an average angular deviation from 90° of 8.0°. The presence of a nitrogen-coordinated ligand will also contribute to the size of the Q_{cc}.

Investigation of an (aryldiazenido)molybdate, **6**, was carried out. Its structure is again similar to that of the (organohydrazido)compounds, the difference being the coordination of two phenyldiazenido groups to each of terminal ligation sites of the octahedral molybdenum nuclei.[45] As seen previously, the resonances due to the two sites are plainly visible in the static powder spectrum (Figure 7a), while the octahedral resonance is shifted to lower shielding. The isotropic chemical shift would be expected to be greater for this species than for the previous two owing to the coordination of two nitrogens per octahedral molybdenum site. However, the solid-state powder line shapes do not demonstrate this fact clearly. The 4.4-kHz MAS spectrum (Figure 7b) plainly shows the narrowed tetrahedral resonance, while the contribution from the octahedral site is somewhat reduced, though visible. In Figure 7c, we present a simulated line shape of the static powder spectrum, and in Figure 7d, we show the devoncolution of the two contributions to the line shape. The sharp, featureless resonance corresponding to the tetrahedral molybdenum sites is caused by a relatively small Q_{cc} of 2.51 MHz, $\eta_Q = 0.16$. The octahedral line shape corresponds to a Q_{cc} of 4.90 MHz, $\eta_Q = 0.19$. The average deviation from the octahedral bond angle, for this species, is 6.8°.

Another (organohydrazido)molybdate of interest is one in which the hydrazines are replaced by a tridentate hydrazidophthalazine (hydralazine) ligand, which coordinates two nitrogens to one of the octahedral sites and one nitrogen to the other octahedral molybdenum site,[45] replacing one of the bridging methoxy groups present in the previous three compounds to give species **7**. It has been found that this causes all four of the molybdenum sites in the species to be NMR inequivalent. In the static powder spectrum (Figure 8a) the contrast between the four possible resonances is not obvious and the octahedral contributions cannot be readily distinguished from the tetrahedral. In the 4.3l-kHz MAS spectrum (Figure 8b), however, one can distinguish the broader octahedral contributions underlying the narrowed tetrahedral contributions. Owing to the lack of any discontinuities, the simulation of this spectrum was not attempted, as a starting guess data set

(46) Shaikh, S. N.; Zubieta, J. *Inorg. Chem.* **1986**, *25*, 4613.

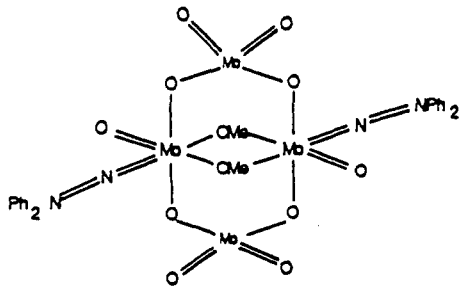

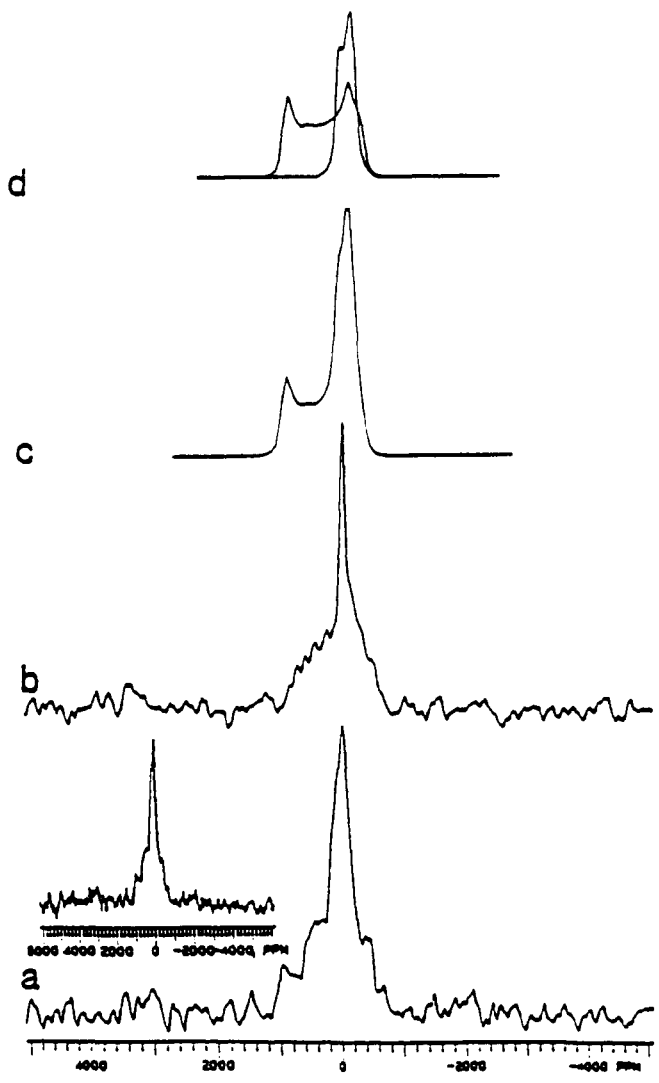

Figure 6. Static powder, MAS, and simulated spectra of a mixed tetrahedral/octahedral molybdenum site species, $[Bu_4N]_2[Mo_4O_{10}(OMe)_2(N_2Ph_2)_2]$ (**5**): (a) static powder spectrum, 64 404 transients, 1-s recycle delay, LB = 3000 Hz; (b) corresponding 3.7-kHz MAS spectrum, 73 240 transients, 1-s recycle delay, LB = 2000 Hz; (c) simulated spectrum; (d) deconvolution of the two contributions to the line shape. Note: The simulated spectra are not on the same scale as the experimental.

for each of the four contributions could not be readily obtained.

Figure 9 shows the static, MAS, and simulated spectra of a purely octahedral molybdenum species, **8**. Species **8** has what is known as the superoctahedral structure, which consists of six octahedra in which one oxygen atom is common to all six octahedra, twelve oxygen atoms are common to two octahedra, and six oxygen atoms are unshared. The six molybdenum centers form the points of the superoctahedral structure.[47] The simulated line

(47) Allcock, H. R.; Bissell, E. C.; Shawl, E. T. *Inorg. Chem.* **1973**, *12*, 2963.

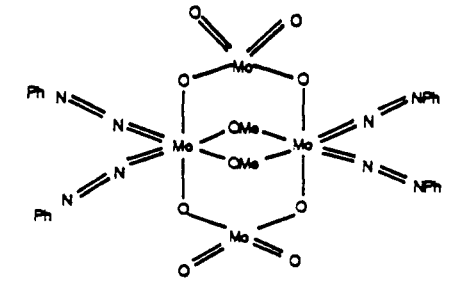

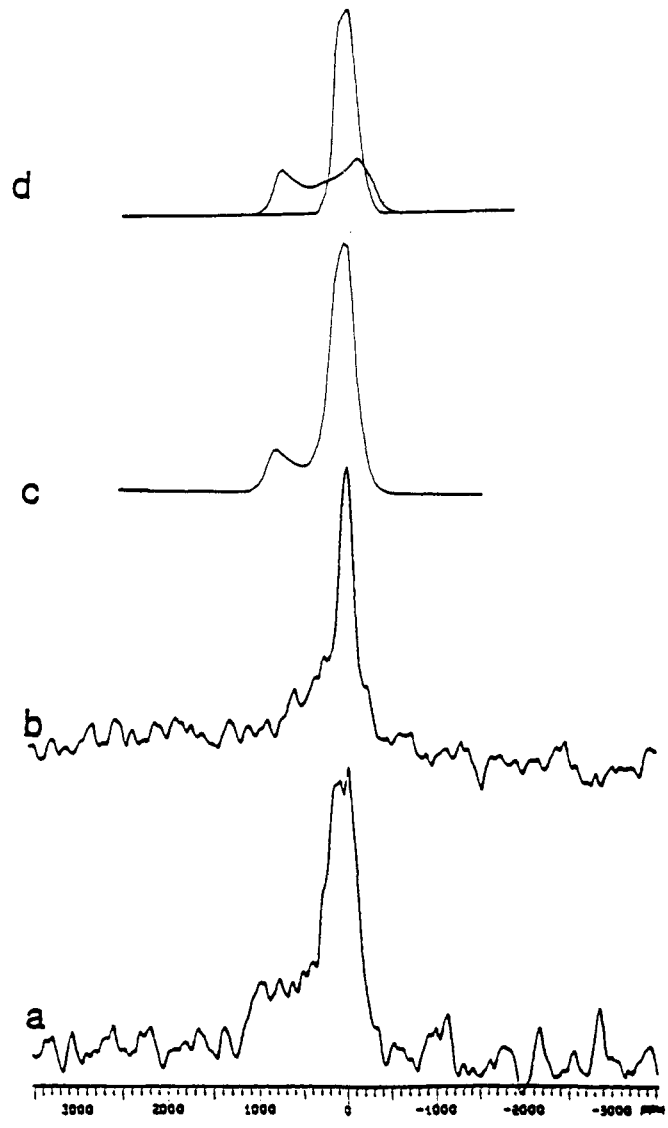

Figure 7. Static powder, MAS, and simulated spectra of a mixed tetrahedral/octahedral site species, $[Bu_4N]_2[Mo_4O_8(OMe)_2(NNPh\text{-}p\text{-}NO_2)_4]$ (**6**): (a) static powder spectrum, 7937 transients, 5-s recycle delay, LB = 3000 Hz; (b) corresponding 4-kHz MAS spectrum, 55 669 transients, 1-s recycle delay; (c) simulated spectrum; (d) deconvolution of the two contributions to the line shape. Note: The simulated spectra are not on the same scale as the experimental.

shape (Figure 9c) yielded the quadrupole and chemical shielding parameters shown in Table II. It should be noted that the inclusion of the Euler angles was essential in this case, as they caused the simultaneous reduction and increase, in intensity, of the singularities at −395 and 505 ppm, respectively. The only explanation we can offer for the relative widths of the singularities of the simulated spectrum being the opposite of the experimental spectrum is that a small amount of impurity is present in the sample, which is contributing a small component to the experimental line shape. The MAS spectrum (Figure 9b) shows that a large value of Q_{cc} is present in this species, leading to a very small narrowing of the spectrum in the MAX experiment.

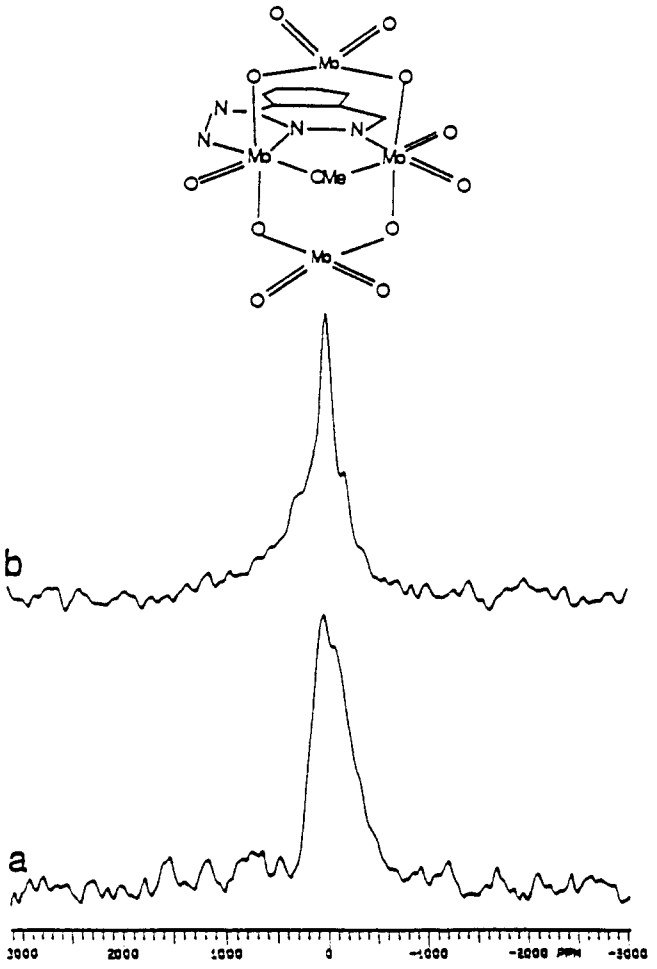

Figure 8. Static powder, MAS, and simulated spectra of a mixed tetrahedral/octahedral species, $[Bu_4N]_2[Mo_4O_{12}(hydralazine)]$ (**7**): (a) static powder spectrum, 27 136 transients, 2-s recycle delay, LB = 300 Hz; (b) corresponding 3.1-kHz MAS spectrum, 221 000 transients, 0.5-s recycle delay, LB = 2000 Hz.

Figure 10 shows the static powder spectrum of species **9**, whose structure is similar to that of species **8**, except for the replacement of one of the Mo(VI)–$O_{terminal}$ groups with a Mo(II)–C_6F_5 group, resulting in a systematic variation of bond lengths around this substitution site. As can be seen, the electronegative nature of this species, the resulting inequivalence of the octahedral molybdenum environments, and the change in the EFG's present in the cluster has caused a dramatic change in the static powder line shape (compare with Figure 9a). From the spectrum we can see more than one contribution to the line shape (from the crystallographic data there are four possible contributions[19]). It is difficult to ascertain if we are observing a resonance from the Mo(II) center; if we are, it may be responsible for the chemically shifted (to lower shielding) component of the line shape. We are, however, definitely observing the convolution of the resonances attributable to the two types of site present in the four Mo(VI) centers adjacent to the Mo(II) site and the Mo(VI) site "opposite" the Mo(II) site. The liquid-state ^{95}Mo NMR[19] spectra revealed a large change in the electron density, or more properly current density, around the Mo(VI) centers, reflected in the greatly changed chemical shifts of these centers.

Figure 11 shows the static powder (Figure 11a), the 4.515-kHz MAS (Figure 11b), and the simulated (Figure 11c,d) spectra of $[Bu_4N]_3[Mo_5O_{16}(OMe)]$[23] (**10**). The structure of this species has been shown to be similar to that of species **2**, consisting of two tetrahedral and three octahedral molybdenum environments. The tetrahedral sites have two bridging (1.806–1.868 Å) and two terminal oxygen bonds (1.709–1.728 Å) and are coordinated in the same positions as the squaric acid ligands in species **2**. Two of the octahedral sites have two terminal oxygen bonds (1.685–1.705 Å), three bridging oxygen bonds (1.915–2.237 Å),

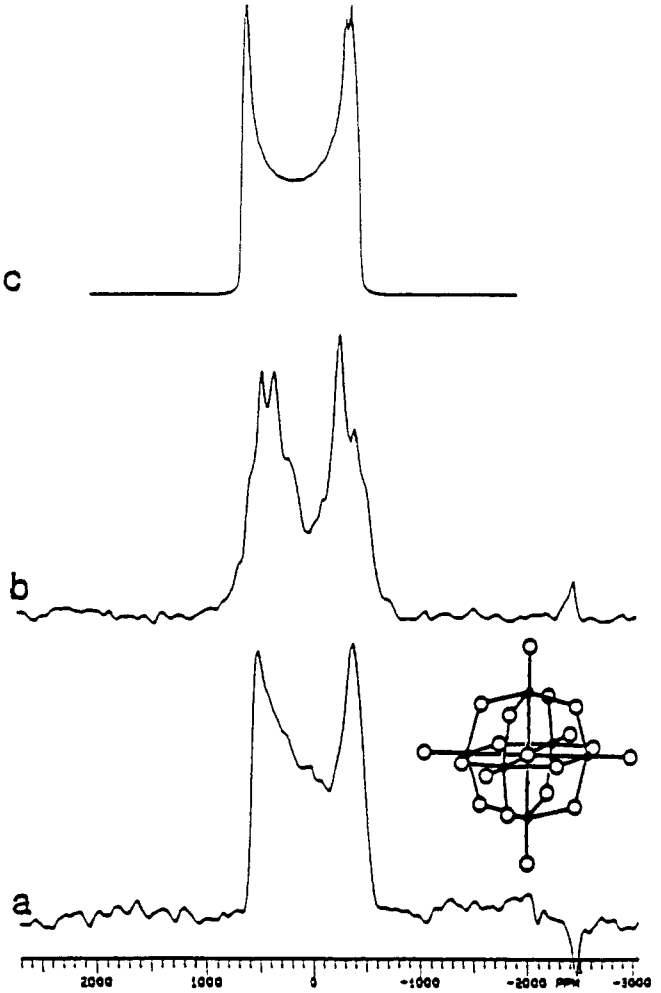

Figure 9. Static powder, MAS, and simulated spectra of the central $\pm^1/_2$ transition of a purely octahedral polyoxomolybdate: (a) static powder spectrum of $[Bu_4N]_2[Mo_6O_{19}]$ (**8**), 32 300 transients, 2-s recycle delay, LB = 2000 Hz; (b) corresponding 3.4-kHz MAS spectrum, 75 000 transients, 2-s recycle delay, LB = 2000 Hz; (c) simulated spectrum obtained from the IGCF program. Note: The simulated spectra are not on the same scale as the experimental.

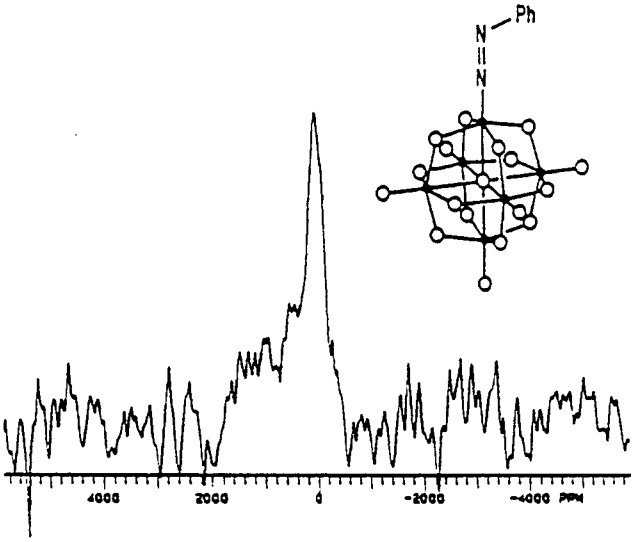

Figure 10. Static powder spectrum of the central $\pm^1/_2$ transition of $[Bu_4N]_3[Mo_6O_{18}(NNC_6F_5)]$ (**9**) (127 680 transients, recycle delay = 1.25 s, LB = 2000 Hz).

and one bridging methoxide bond (2.285 Å), while the other octahedral molybdenum site has one terminal oxygen bond (1.688 Å), four bridging oxygen bonds (1.795–2.082 Å), and a single bridging methoxide bond (2.446 Å).[23] Although crystallo-

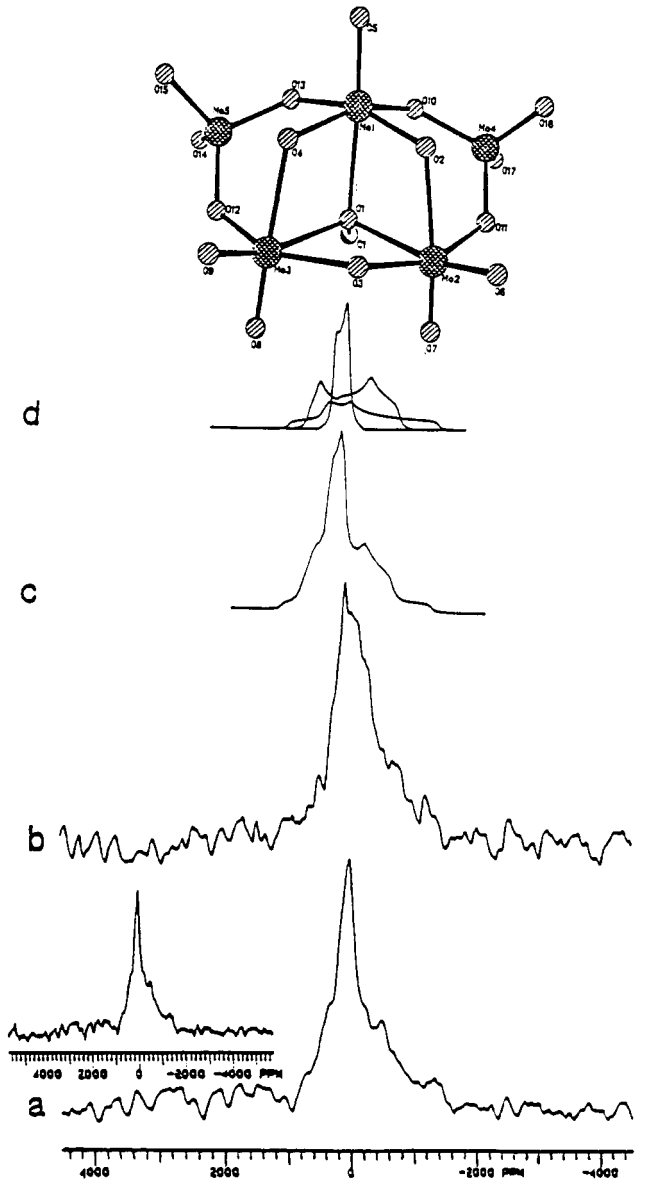

Figure 11. Static powder, MAS, and simulated spectra of the central $\pm^1/_2$ transition of $[Bu_4N]_3[Mo_5O_{16}(OMe)]$ (**10**): (a) static powder spectrum, 58 604 transients, recycle delay = 1.2 s, LB = 2500 Hz; (b) 4.515-kHz MAS spectrum, 48 000 transients, recycle delay = 1.2 s, LB = 2500 Hz; (c) simulated spectrum; (d) deconvolution of the three contributions to the line shape. Note: The simulated spectra are not on the same scale as the experimental.

graphically there are five inequivalent molybdenum environments, in our NMR experiment we can only approximate the line shape by assuming there are three contributions to the line shape. The two tetrahedral molybdenums are responsible for the sharp central resonance at 5 ppm. This resonance corresponds to a Q_{cc} of 2.17 MHz, η_Q = 0.07. As the two octahedral sites with two terminal oxygen bonds have a greater degree of freedom, they will tend to be less distorted from true octahedral symmetry than the single octahedral site with only one terminal oxygen bond, and we will correlate these sites with a smaller Q_{cc}. This "degree of freedom" argument is again reinforced by the angular deviation from octahedral symmetry observed at each site, from the crystallographic data. The single octahedral site with one terminal bond has an average deviation from the expected 90° octahedral angle of 10.5°, while the deviations for the two octahedral sites with two terminal bonds are only 9.6 and 9.7°. The deconvolution of the three contributions to the line shape has yielded two resonances attributable to the octahedral sites; the lowest Q_{cc} is one of 5.46 MHz with a corresponding η_Q value of 0.32, while the higher Q_{cc} value of 5.52 MHz, corresponding to the octahedral site with one terminal oxygen atom, has a corresponding η_Q value of 0.80. This

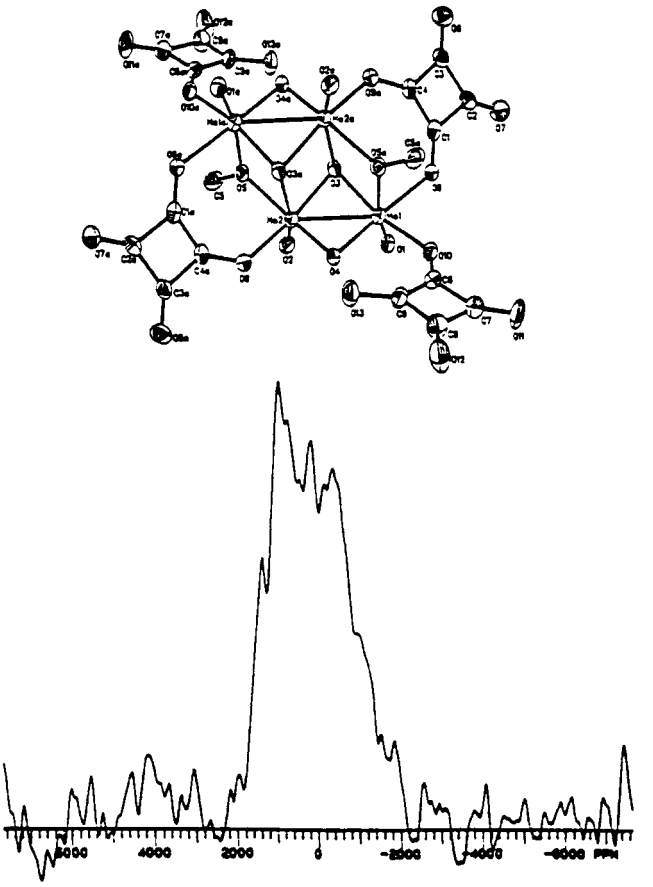

Figure 12. Static powder spectrum of the central $\pm^1/_2$ transition of $[Bu_4N]_4[Mo_4O_8(OMe)_2(C_4O_4)_4]$ (**11**) (95 425 transients, recycle delay = 1.2 s, LB = 4500 Hz).

assignment is not convincing on the basis of only the distortion argument, as the Q_{cc} values are very similar. However, the intensities of the two octahedral components yield the same assignment, assuming that the species was allowed to experience a $5T_1$ recycle delay.

This assignment is also supported when compared with the simulation results obtained on species **2**. Of interest in the spectra of species **10** and species **2** is the fact that, in the case of species **2**, the two octahedral components observed in the line shape of species **10** have values of η_Q very similar to those observed for species **2**. This indicates that they possess similar distorted environments as well as similar symmetries. The line shape of **10** clearly demonstrates the presence of two resonances due to the two different octahedral sites as well as a resonance taken as being caused by two equivalent tetrahedral molybdenum sites. It is interesting to note, however, that the Q_{cc} values of the octahedral sites in species **10** have increased from those observed in species **2**. Chen et al.[23] have discussed the similarities of the $[MoO_4]^{2-}$ and $[C_4O_4]^{2-}$ ligands that lead to successful substitution of these two species for each other without causing any structural change. However, our experiments seem to indicate that substitution of $[MoO_4]^{2-}$ for $[C_4O_4]^{2-}$ leads to a significant change in the size of the EFG in the electronic environments around the two different types of octahedral molybdenum, while the symmetry of the EFG remains almost unchanged. There also seems to be an increase in the structural distortion that seems to be restricted to only one of the octahedral sites and is responsible for the increase of the Q_{cc} value of that site to 5.52 MHz. The site likely to be most affected by the substitution of the squaric acid ligands with molybdate ligands is the single disubstituted molybdenum site. Thus we can assign the 5.52-MHz resonance to this site and the 5.46-MHz resonance to the two monosubstituted sites.

One of the few heptacoordinate species that we looked at was $[Bu_4N]_4[Mo_4O_8(OMe)_2(C_4O_4)_4]\cdot MeOH$[25] (**11**). Figure 12 shows the static powder spectrum of this compound. Crystallographi-

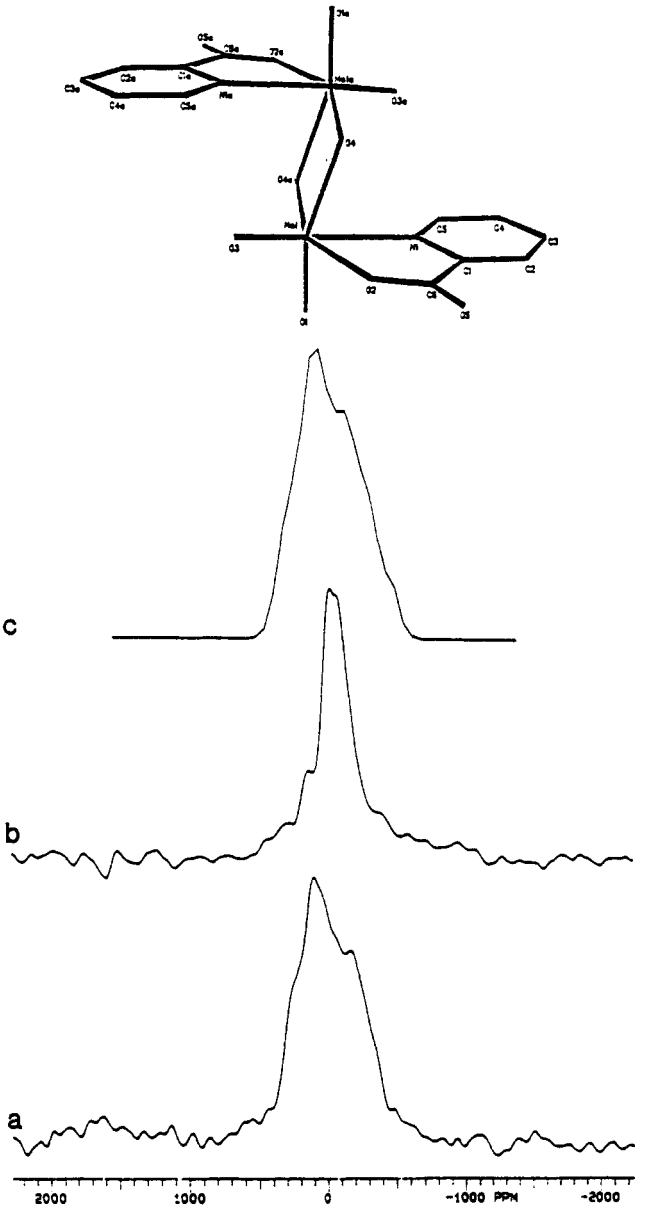

Figure 13. Static powder, MAS, and simulated spectra of the central $\pm^1/_2$ transition of $[Bu_4N]_2[Mo_2O_6(C_5H_4N\text{-}2\text{-}COO)_2]$ (**12**): (a) static powder spectrum, 45 061 transients, recycle delay = 1 s, LB = 2000 Hz; (b) 4.28-kHz MAS spectrum, 55 018 transients, recycle delay = 1 s, LB = 2000 Hz; (c) simulated spectrum. Note: The simulated spectra are not on the same scale as the experimental.

cally, and in the NMR experiment, there are two inequivalent molybdenum sites in the ratio 1:1. The powder spectrum is quite broad, maybe due to the presence of Mo–Mo bonds and a low degree of symmetry in these heptacoordinate species. Simulation of the line shape was not attempted owing to the singal-to-noise level of the spectrum although an estimate of the Q_{cc} values of the two sites would put them in the 5.5–6.7-MHz range.

Another octahedrally coordinated species that we have investigated is $[Bu_4N]_2[Mo_2O_6(C_5H_4N\text{-}2\text{-}CO_2)_2]$[26] (**12**). Each of the two equivalent molybdenum sites consists of two terminal oxygen bonds (1.709–1.713 Å), two bridging oxygens between the two molybdenum sites (2.225 Å), a bridging oxygen coordinated from the carbonyl group (2.139 Å), and a coordinated pyridine nitrogen bond (2.382 Å). The pyridine ligands are in a trans conformation. Figure 13a shows the static powder spectrum of this spcecies. The simulation of the static powder spectrum (Figure 13c) corresponds to a Q_{cc} value of 3.20 MHz, $\eta_Q = 0.64$, $\sigma_{11} = -139$ ppm, $\sigma_{22} = 173$ ppm, $\sigma_{33} = 175$ ppm, $\alpha = 34°$, $\beta = 28°$, and $\gamma = -28°$. The narrowing of the resonance in the 4.28-kHz MAS spectrum (Figure 13b) demonstrates the existence of a considerable chemical shielding interaction in comparison with the size of Q_{cc}. This is

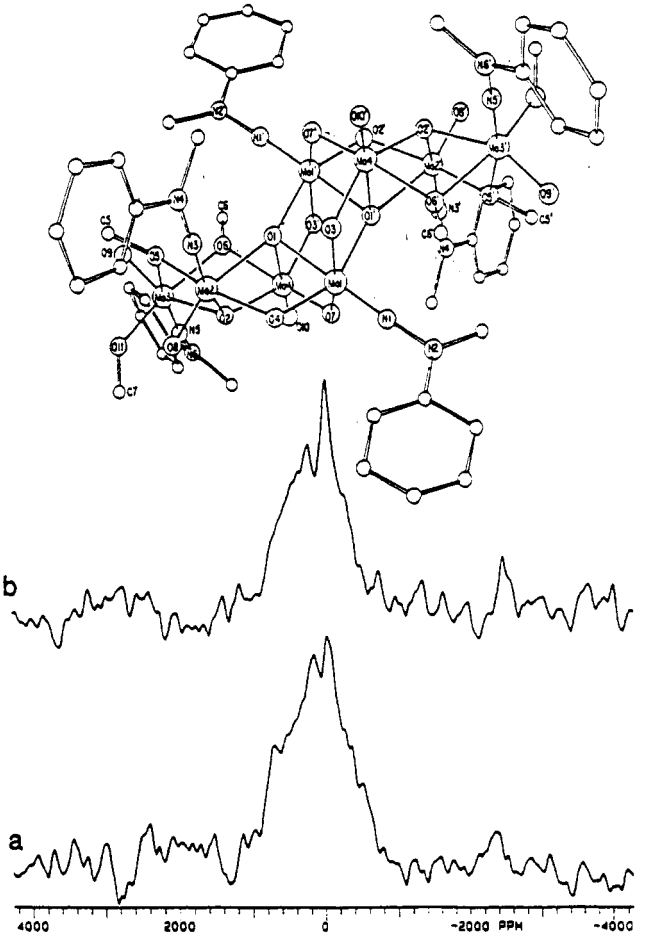

Figure 14. Static powder, MAS, and simulated spectra of the central $\pm^1/_2$ central transition of $[Bu_4N]_2[Mo_8O_{16}(OMe)_6(N_2MePh)_6]$ (**13**): (a) static powder spectrum, 100 000 transients, recycle delay = 1 s, LB = 2500 Hz; (b) 4.116-kHz MAS spectrum, 85 153 transients, recycle delay = 1 s, LB = 2500 Hz.

in agreement with our simulated results.

Finally, a rather complex species was investigated that contained four nonequivalent octahedral molybdenum environments: $[Bu_4N]_2[Mo_8O_{16}(OMe)_6(N_2MePh)6]$[19] (**13**). The static powder spectrum is shown in Figure 14a. There are four contributions to this line shape; however, only two can be discerned from inspection. Thus, no attempt was made to simulate this spectrum, as any number of fits could be accomplished on the basis of the spectrum. The fact that the 4.12-kHz MAS spectrum (Figure 14b) shows little narrowing indicates that all four contributions have quite large values of Q_{cc} (~4–5 MHz) in comparison to any chemical shielding interaction.

Summary

In this investigation we have demonstrated the feasibility of using solid-state ^{95}Mo NMR spectroscopy to obtain important structural information such as the values of Q_{cc} and η_Q, as well as some idea of the chemical shielding interaction present when the chemical shielding and quadrupolar interactions are on the same order of magnitude. We were able to distinguish between octahedral and tetrahedral sites as well as distinguish between different octahedral sites in the same molecule by comparison of our simulation data and the crystallographic structural details. We have also demonstrated the relationship between the degree of distortion present in the octahedral environment and the value of Q_{cc}. The changes in the electronic environments of the individual molybdenum centers are also apparent in these experiments and may aid in an understanding of the electronic effects of substitution of different ligands and variation of the position of substitution. In general, the results obtained were similar to the results of the liquid-state NMR spectroscopy for these compounds.[19] It is important to note, however, that more information

Table III. Electric Field Gradient, Charge Density, and Bond Distance Summary for the $[MoO_6]^{6-}$ Anion

r_{Mo-O}, Å	$q_{O,axial}$	$q_{O,base}$	q_{Mo}	q_{zz}[a]	$q_{zz,nucl}$[a]
1.90	−0.942 390	−1.026 978	−0.007 309	0.483 407	−0.015 709
2.00	−0.965 484	−1.004 985	−0.049 092	0.159 332	−0.007 212
2.10	−0.983 993	−0.983 993	−0.096 041	0.000 000	0.000 000
2.20	−0.994 509	−0.965 646	−0.148 397	−0.051 737	0.006 444
2.30	−0.995 736	−0.951 437	−0.202 782	−0.063 718	0.011 239

[a] The units for the field gradient are atomic units. They can be converted to Q_{cc} values in MHz by the following equation: $Q_{cc} = q_{zz}(e^2Q/a_0^3h) = q_{zz} \times 28.196$ MHz.

is obtained in the solid-state experiments. In the liquid state, it was possible to distinguish between tetrahedral and octahedral sites on a chemical shift and line width basis. The individual octahedral sites could not be distinguished. In some cases the octahedral sites could not be seen in the spectrum, possibly due to the presence of a large Q_{cc} value causing rapid relaxation. In the solid-state experiment, not only were we able to distinguish between octahedral and tetrahedral sites, but we were also able to distinguish between the individual octahedral sites and make assignments on the basis of the simulated line shape results and the average bond angle deviation from the expected octahedral bond angle, obtained from the available crystallographic data. It has been noted that the asymmetry parameter is also a reliable tool for assignment.[48] With the exception of the symmetric species $[Mo_6O_{19}]^{2-}$, there appears to be a definite difference in the η_Q value obtained for those octahedral molybdenums with two nonbridging oxygen atoms (η_Q is small to medium) and those with one or zero nonbridging oxygen atoms (η_Q is close to 1). On the basis of this correlation, one's assignments will coincide with those made in this work. The solid-state experiment also has the advantage of seeing resonances from all the sites; i.e., resonances of sites with large values of Q_{cc} are not missing due to the absence of large-scale molecular motion, which can give rise to an effective quadrupolar relaxation mechanism.

It is hoped that this investigation will lead to an extension of the field of solid-state ^{95}Mo NMR spectroscopy to the important catalytic and biological systems in which molybdenum is found. Liquid-state ^{95}Mo NMR studies will be done on any uninvestigated species in order to support our conclusions and yield better chemical shift information on these species.

Acknowledgment. We acknowledge the partial support of this research by the National Science Foundation via Grants CHE85-44272 and CHE86-11306 and the National Institutes of Health via Grant GM26295. The work performed in the laboratory of J.Z. was supported by the National Science Foundation via Grant CHE8815299. We also thank one of the reviewers for his useful comments.

Appendix

In this report and others,[20,21] we have described the quadrupole coupling constant, Q_{cc}, as being sensitive to the degree of distortion about the molybdenum center. It is our intent here to discuss this assertion more completely.

The nuclear quadrupole coupling constant is parametrically dependent upon the zz component of the electric field gradient tensor, q, i.e. (e^2Qq_{zz}/h). The other symbols, e, Q, and h are the charge of the electron, the quadrupole moment of the nucleus of interest, and Planck's constant, respectively. The zz element of the field gradient tensor can be expressed as[49]

$$q_{zz}^{I} = \sum_{K} Z \frac{2Z_{IK}Z_{IK} - (X_{IK}^2 + Y_{IK}^2)}{R_{IK}^5} - \sum_{k}\sum_{l} P_{kl}\left\langle \chi_k \frac{|2z_Iz_I - (x_I^2 + y_I^2)|}{r_I^5} \chi_l \right\rangle \quad \text{(A1)}$$

The first summation extends over the number of atoms, whereas the double summation is over the number of basis functions. Further, the uppercase symbols X_{IK}, Y_{IK}, and Z_{IK} refer to the nuclear coordinates associated with the vector from nucleus I to nucleus K. The lower case symbols x_I, y_I, and z_I refer to the components of the vector from the nucleus I to the electron. Z_K denotes the nuclear charge on atom K. The symbols P_{kl}, χ_k, and χ_l refer to the kl element of the density matrix and basis functions k and l, respectively. The symbols R_{IK} and r_I refer to the scalar internuclear distance between nuclei I and K and the distance to the electron and nucleus I, respectively. We will refer to the two terms in eq A1 as the nuclear and electronic terms for the first and second terms, respectively.

From the form of the gradient operator, it is clear that for systems of O_h symmetry q_{zz} will be zero. This is due to the isotropy of the space: the integrals over $x_Ix_I(r_I^{-5})$, $y_Iy_I(r_I^{-5})$, or $z_Iz_I(r_I^{-5})$ will be equal. Likewise, the geometrical factors in the first term of eq A1 will zero for the same reasons. However, for the discussion here it is the distortion from O_h symmetry that is of interest. The simplest type of distortion is a uniaxial distortion, that is, a symmetric contraction or elongation of a single axis. To illustrate the consequences of such a distortion, we have performed a series of ab initio[43] calculations on the $[MoO_6]^{6-}$ anion, the results of which are summarized in Figure 2 and Table III.

The first point to be discussed is which term in eq A1, if any, makes the dominant contribution to q_{zz}. To address this question, we have summarized the values of the total q_{zz} and the values of $z_{zz,nucl}$ calculated from the geometry and the total charges. It is clear from Table III that the nuclear contributions are small in comparison to the electronic contributions, i.e. the second term in eq A1.

In the analysis of the electronic term, we, as others[50] have, will make some simplifying assumptions. First, we need only focus on the valence orbitals, i.e. ignore any anisotropy in the elements of the density matrix for filled orbitals. Second, the ns orbital (in fact any spherically symmetric orbital) will make no contributions to the field gradient. Even with these simplifications, the problem is still complex. It is evident from the symmetry, D_{4h}, of the distorted $[MoO_6]^{6-}$ anion that the valence orbital block of the density matrix associated with the molybdenum atom is diagonal. Hence, the contribution to q_{zz} arising from molybdenum orbitals comes from the charge anisotropy on the molybdenum atom. As a result, there should be dependence of the field gradient tensor on the total charge on the molybdenum. The situation with the oxygen atom contributions is more complicated. However, one would also predict a relationship between the charge density on the oxygen atoms as well. Examination of Table III supports this qualitative reasoning. That is, in the most contracted Mo–O bond distance, 1.9 Å, the axial oxygen atoms are their most positive (−0.942 390), while at the most elongated distance of 2.3 Å the axial oxygen atoms are the most negative (−0.995 736). A similar pattern is exhibited by the molybdenum atom. The opposite trend is manifested by the in-plane or basal oxygen atoms. This is, when the axial oxygen atoms are at the shortest Mo–O bond distance, the basal oxygens are the most negative (−1.026 978). Likewise, when the axial Mo–O bond is longest, the basal oxygen atoms have become more positive (−0.951 437). Hence, there appears to be a charge flow from the basal oxygens through the molybdenum atom to the axial oxygens as one goes from a short axial Mo–O bond to a long Mo–O bond. Similar correlations between orbital charge density and q_{zz} can be extracted from the angular distortions Figure 2b.

From the form of the field gradient operator, q_{zz} is a measure of the charge anisotropy at a particular center. In systems with distorted O_h or T_d symmetry, q_{zz} should mirror those distortions. Hence, Q_{cc} should be an accurate reflection of the degree of distortion about such a center.[44]

(48) We acknowledge one of the reviewers for this observation.

(49) Kern, C. W.; Karplus, M. *J. Chem. Phys.* **1965**, *42*, 1062.
(50) Townes, C. H.; Dailey, B. P. *J. Chem. Phys.* **1949**, *17*, 782.